Lecture 1:

1.1 An Introduction to Radio Astronomy

1.1.1 What is Radio Astronomy?

Radio astronomy is the study of natural radio emission from celestial sources.
The radio frequency range is defined by the atmosphere and by quantum noise
$10 \text{ MHz} \lesssim \nu \lesssim 1 \text{ THz}$

1.1.2 Atmospheric Windows

The visible light window covers $3000 \text{ K} \lesssim T \lesssim 10,000 \text{ K}$ blackbody stars, gas ionized by
stars, galaxies of stars, planets reflecting starlight
Blackbody stars are weak radio sources
The radio window is bounded by ionospheric refraction,
absorption by rotating and vibrating polar molecules
Radio opacity from dry air, O_2, hydrosols, water vapor line and continuum
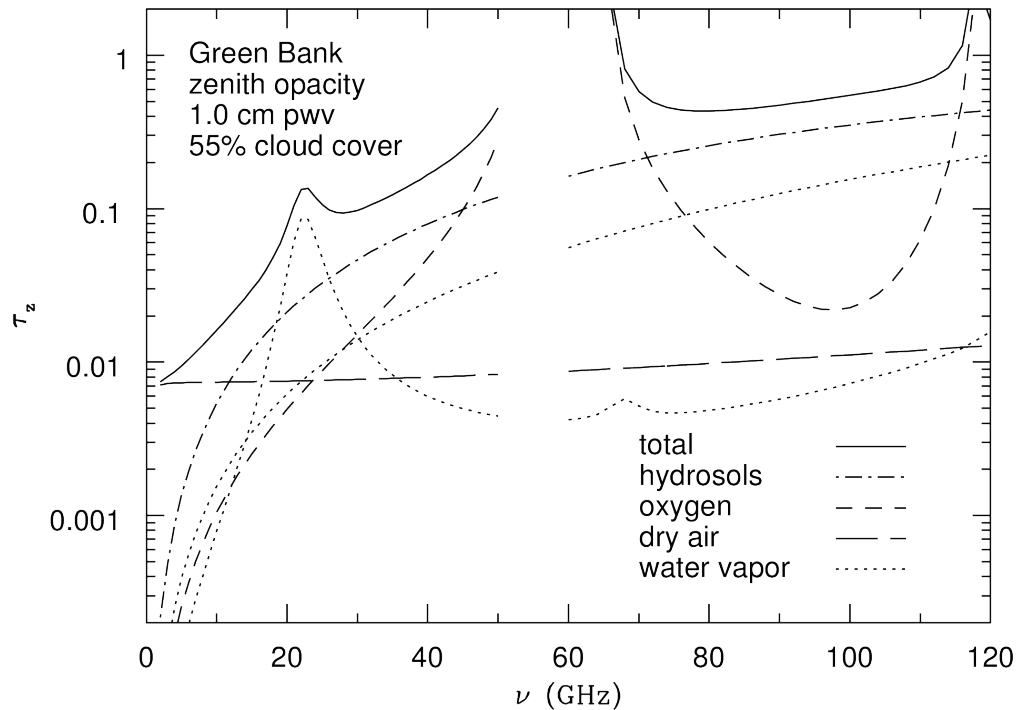Radio refraction by water vapor is large

Fig. 1.— The atmospheric zenith opacity τ_z at Green Bank during a typical summer night.
The oxygen and dry-air opacities are nearly constant, while the water vapor and hydrosol
contributions vary significantly with weather.

1.1.3 Astronomy in the Radio Window

The radio window is broad (5 decades of frequency),
includes most astronomical objects, emission mechanisms, and propagation phenomena,
and requires a wide range of radio telescopes and observing techniques

The radio window was opened before space astronomy, leading to many major discoveries:
violent phenomena, often powered by gravity, cosmologically distant, very cold
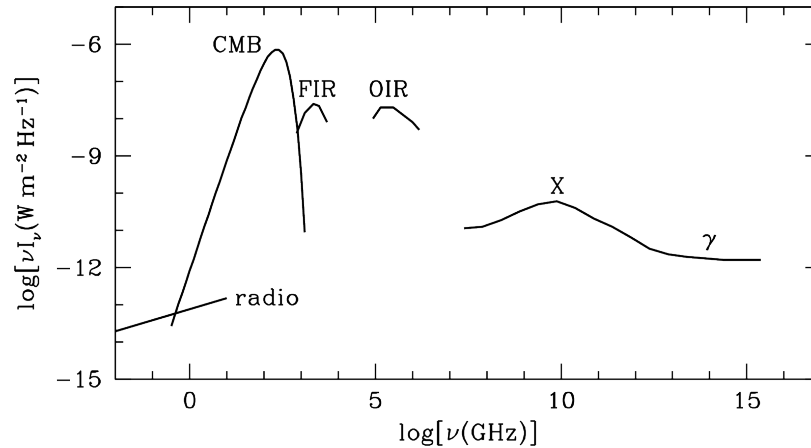Radio emission is usually energetically insignificant

Fig. 2.— The electromagnetic spectrum of the universe at radio, far-infrared (FIR), optical/near-infrared (OIR), and X-ray (X) and gamma-ray (γ) frequencies.

1.1.4 Long Wavelengths and Low Frequencies

Long wavelengths are unbiased by dust, allow coherent emission by groups of charged particles
Low photon energies $E = h\nu \ll kT$
Thermal emission $B_\nu = 2kT\nu^2/c^2$ visible even from cold objects
Stimulated emission, astrophysical masers exist
Radio sources can remember the past
Plasma effects (scattering, dispersion, Faraday rotation, ...) $\propto \nu^{-2}$.

1.1.5 Radio Telescopes and Aperture-Synthesis Interferometers

Diffraction-limited resolution $\theta \approx \lambda/D$
Aperture-synthesis interferometers
Sensitive coherent interferometers limited to radio by quantum noise $T \approx h\nu/k$
Interferometers: Large $D \sim 10^4$ km, small θ,
Accurate astrometry (clocks are better than rulers),
High dynamic range and image fidelity with self-calibration

Lecture 2:

1.2 Discovery of Cosmic Radio Noise

Astronomers knew that blackbody stars would be undetectably weak radio sources

$$B_\nu(\nu, T) = \frac{2h\nu^3}{c^2} \frac{1}{\exp\left(\dfrac{h\nu}{kT}\right) - 1} \approx \frac{2kT\nu^2}{c^2} \ , \quad \frac{h\nu}{kT} \sim 10^{-5} \ll 1 \tag{1}$$

Note subscript ν and argument ν, define constants and variables
CGS and SI (MKS) units, "astronomical" units, constants in Appendix F.
Read Appendix F.
Dimensional analysis, dictionary of symbols in Appendix G.

Jansky (1932) accidentally discovered continuum emission our Galaxy
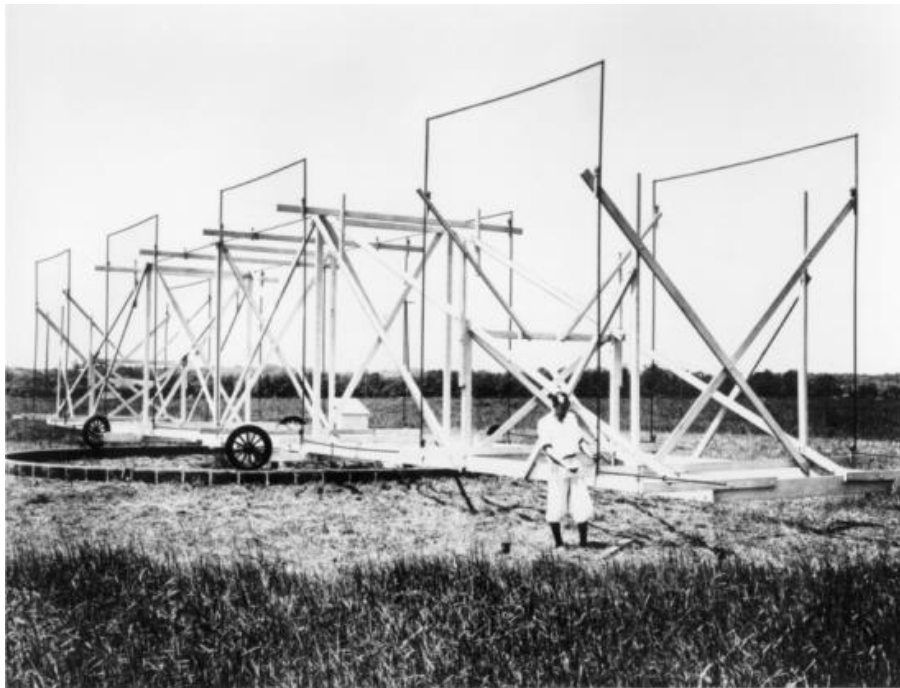

Fig. 3.— Karl Jansky and the antenna that discovered cosmic radio static.

Grote Reber (1938) built a 10 m parabolic radio telescope, mapped the Galaxy at 160 MHz, and showed it has a nonthermal spectrum.

1.3 A Tour of the Radio Universe

Parallel universes of optical and radio astronomy
Radio-faint optical objects, optically faint radio sources
Familiar optical objects may look different at radio wavelengths

Radio sky is black in daytime, clouds emit, planets emit

Galactic continuum from massive short-lived stars and SNRs

Powerful radio galaxy Cyg A $z \approx 0.057$, $d \approx 240$ Mpc, radio $L \sim 10^{45}$ erg s^{-1}, easily visible anywhere in the universe, extent $D \sim 100$ kpc,

3C 273 quasar $z \approx 0.16$.

Cosmic Microwave Background (CMB) radiation

See also: `https://www.cv.nrao.edu/course/astr534/Tour.html`

Fig. 4.— Grote Reber's backyard radio telescope in Wheaton, IL. The parabolic reflector is about 10 m in diameter.

Lecture 3:

2.1 Brightness and Flux Density

Ray-optics approximation in vacuum
spectral brightness (specific intensity)

$$I_\nu \equiv \frac{dP}{(\cos\theta\, d\sigma)\, d\nu\, d\Omega} \quad (\text{W m}^{-2}\text{ Hz}^{-1}\text{ sr}^{-1}) \tag{2}$$

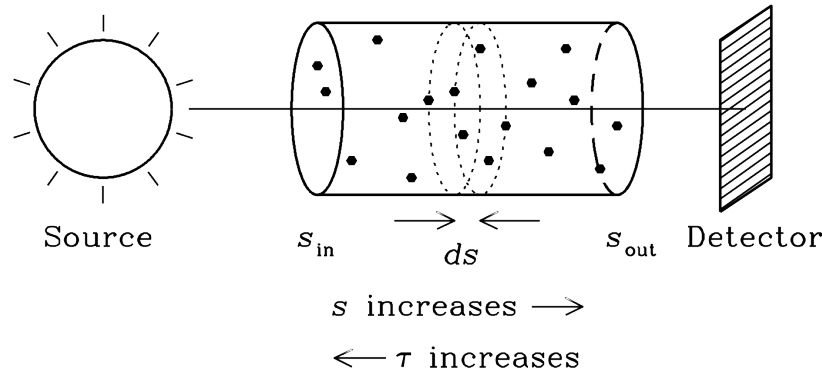$$|I_\nu\, d\nu| = |I_\lambda\, d\lambda| \tag{3}$$

Specific intensity is conserved along a ray in empty space
Flux density is specific intensity integrated over source solid angle

$$S_\nu \equiv \int_{\text{source}} I_\nu(\theta,\phi)\cos\theta\, d\Omega \approx \int_{\text{source}} I_\nu(\theta,\phi)\, d\Omega \tag{4}$$

Inverse square law, spectral luminosity

$$lL_\nu = 4\pi d^2 S_\nu \tag{5}$$

2.2 Radiative Transfer

Source s_{in} ds s_{out} Detector

s increases $\longrightarrow$

$\longleftarrow \tau$ increases

(linear) Absorption coefficient:

$$\kappa \equiv \frac{dP}{ds} \qquad \frac{dI_\nu}{I_\nu} = -\kappa\, ds \tag{6}$$

$$\frac{I_\nu(s_{\text{out}})}{I_\nu(s_{\text{in}})} = \exp\left[-\int_{s_{\text{in}}}^{s_{\text{out}}} \kappa(s')\, ds'\right] \tag{7}$$

$$\tau \equiv -\int_{s_{\text{out}}}^{s_{\text{in}}} \kappa(s')\, ds' \quad \text{so} \quad \frac{I_\nu(s_{\text{out}})}{I_\nu(s_{\text{in}})} = \exp(-\tau) \tag{8}$$

Emission coefficient

$$j_\nu \equiv \frac{dI_\nu}{ds} \tag{9}$$

Radiative transfer equation

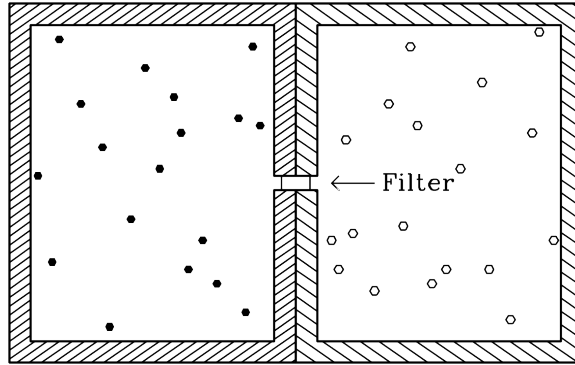$$\frac{d\,I_\nu}{ds} = -\kappa I_\nu + j_\nu \tag{10}$$

Fig. 5.— Kirchhoff's thought experiment invokes two cavities in thermodynamic equilibrium connected through a filter that passes radiation in the narrow frequency range ν to $\nu + d\nu$. The cavities may be made of different materials and contain different emitting/absorbing particles.

Kirchhoff's law in LTE at temperature T:

$$\frac{j_\nu(T)}{\kappa(T)} = B_\nu(T) \tag{11}$$

Rayleigh-Jeans brightness temperature is *defined* by

$$T_{\rm b} \equiv \frac{I_\nu c^2}{2k\nu^2} \tag{12}$$

and this *definition* applies for *any* I_ν, ν.

Kirchhoff's law for opaque bodies in LTE at temperature T:

$$e(\nu) = a(\nu) = 1 - r(\nu) \tag{13}$$

so

$$T_{\rm b} = a(\nu)T = [1 - r(\nu)]T \tag{14}$$
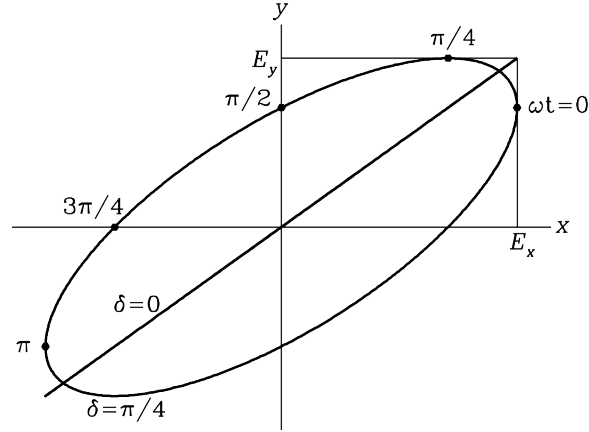
Lecture 4:

2.3 Polarization

Fig. 6.— The electric field vector of any monochromatic wave traveling in the $\hat{z}$-direction pointing up out of the page traces an ellipse that can be written in the form $\vec{E} = [\hat{x}E_x \exp(i\phi_x) + \hat{y}E_y \exp(i\phi_y)] \exp[i(\vec{k} \cdot \hat{z} - \omega t)]$. The ellipse shown has $\delta = +\pi/4$ and $E_x/E_y = 1.4$. If $\delta \equiv \phi_x - \phi_y = 0$, the ellipse becomes a line, while a $\delta = \pm\pi/2$, $E_x = E_y$ would make it a circle. When $\delta > 0$, the tip of the vector rotates clockwise as viewed from the source below the page and counterclockwise as seen by an observer above the page, as shown by the time samples at $\omega t = 0, \pi/4, \pi/2, \ldots$.

The polarization of an astronomical source can very rapidly with time. Its time-averaged polarization can be described by the Stokes parameters:

$$I \quad = \langle E_x^2 + E_y^2 \rangle / R_0, \tag{15}$$
$$Q \quad = \langle E_x^2 - E_y^2 \rangle / R_0, \tag{16}$$
$$U \quad = \langle 2E_x E_y \cos\delta \rangle / R_0, \tag{17}$$
$$V \quad = \langle 2E_x E_y \sin\delta \rangle / R_0, \tag{18}$$

where the brackets indicate time averages, R_0 is the radiation resistance of free space, and I is the total flux density, regardless of polarization. The polarized flux density is

$$I_{\rm p} = (Q^2 + U^2 + V^2)^{1/2} \tag{19}$$

and the degree of polarization is defined as

$$p \equiv \frac{I_{\rm p}}{I} \ . \tag{20}$$

2.4 Blackbody Radiation

Blackbody radiation = cavity radiation = equilibrium radiation

The Rayleigh-Jeans derivation counts all standing-wave modes and assigns average energy $\langle E \rangle = kT$ to each, yielding the Rayleigh-Jeans approximation for the spectral brightness of blackbody radiation

$$B_\nu = \frac{2kT\nu^2}{c^2} = \frac{2kT}{\lambda^2} \qquad (h\nu \ll kT) . \tag{21}$$

The Planck derivation differs in quantizing the radiation energy per mode to integer multiples of $E = h\nu$ = photon energy. This yields

$$B_\nu = \frac{2kT\nu^2}{c^2} \left[\frac{\frac{h\nu}{kT}}{\exp\left(\frac{h\nu}{kT}\right) - 1} \right] , \tag{22}$$

where the first factor is the Rayleigh-Jeans approximation and the quantity in square brackets is the quantum correction factor. Planck's equation is usually written in the simpler form

$$B_\nu(\nu, T) = \frac{2h\nu^3}{c^2} \frac{1}{\exp\left(\frac{h\nu}{kT}\right) - 1} . \tag{23}$$

Integrating Planck's law over all frequencies gives the Stefan–Boltzmann law for the total intensity

$$B(T) \equiv \int_0^\infty B_\nu(T)d\nu = \frac{\sigma T^4}{\pi} \quad \text{where} \quad \sigma \equiv \frac{2\pi^5 k^4}{15c^2 h^3} \approx 5.67 \times 10^{-5} \frac{\text{erg}}{\text{cm}^2 \text{ s K}^4 \text{ (sr)}} . \tag{24}$$

The total radiation energy density

$$u \equiv \int_0^\infty u_\nu d\nu = \frac{4\pi I}{c} = \frac{4\sigma T^4}{c} \tag{25}$$

for blackbody radiation. The spectral flux density emitted from the surface of an isotropic source is

$$F_\nu = \int I_\nu \cos\theta \, d\Omega = \pi I\nu . \tag{26}$$

The total flux, or power per unit area, emitted by a blackbody at temperature T is

$$F(T) = \pi B(T) = \sigma T^4 . \tag{27}$$

Lecture 5:

2.5 Noise Generated by a Warm Resistor

Fig. 7.— Two resistors connected by a lossless transmission line of length $a \gg \lambda$, the longest wavelength of interest. In equilibrium, the transmission line can support only those standing waves having zero voltages at the ends; other modes are suppressed by the lossy resistors.

A warm resistor is the 1D analog of a 3D blackbody. In equilibrium at temperature T it generates noise with spectral power (Nyquist formula)

$$P_\nu = kT \qquad (h\nu \ll kT) . \tag{28}$$

The "noise temperature" is *defined* by

$$T_{\mathrm{N}} = \frac{P_\nu}{k} . \tag{29}$$

At any frequency, the exact form of the Nyquist formula is

$$P_\nu = kT \left[\frac{\dfrac{h\nu}{kT}}{\exp\!\left(\dfrac{h\nu}{kT}\right) - 1} \right] = \frac{h\nu}{\exp\!\left(\dfrac{h\nu}{kT}\right) - 1} . \tag{30}$$

2.6 Cosmic Microwave Background (CMB) Radiation

In the homogeneous expanding universe, the Hubble parameter is defined by

$$H \equiv \lim_{d \to 0} \left(\frac{v}{d} \right) . \tag{31}$$

and its present value is $H_0 \approx 67.8 \pm 0.9$ km s^{-1} Mpc^{-1}. The Hubble time is defined by $t_{\mathrm{H}} \equiv H_0^{-1} \approx 4.55 \times 10^{17}$ s $/ 10^{7.5}$ s yr$^{-1} \approx 1.44 \times 10^{10}$ yr and the Hubble distance is defined by $d_{\mathrm{H}} = c/H_0 \approx 1.36 \times 10^{28}$ cm $\approx 4.4 \times 10^9$ pc $\approx 1.4 \times 10^{10}$ light years.
The critical density is

$$\rho_{\mathrm{c}} = \frac{3H_0^2}{8\pi G} \approx 8.6 \times 10^{-30} \text{ g cm}^{-3} \tag{32}$$

for $H_0 = 67.8$ km s^{-1} Mpc^{-1}.

The universe is filled with blackbody radiation at temperature $T_0 \approx 2.73$ K today. In the past the CMB temperature was $T = T_0(1 + z)$, where the redshift z is defined by

$$z \equiv \frac{\lambda_\mathrm{o} - \lambda_\mathrm{e}}{\lambda_\mathrm{e}} = \frac{\lambda_\mathrm{o}}{\lambda_\mathrm{e}} - 1 = \frac{\nu_\mathrm{e}}{\nu_\mathrm{o}} - 1 \ . \tag{33}$$

The redshift z and universal expansion factor a are related by $(1 + z) = a^{-1}$.
The CMB comes from $z \approx 1091$, when the age of the universe was $t_* \approx 379,000$ yr.
See "ΛCDM Cosmology for Astronomers," Condon & Matthews 2018, PASP, 130:073001.

Big-bang nucleosynthesis.

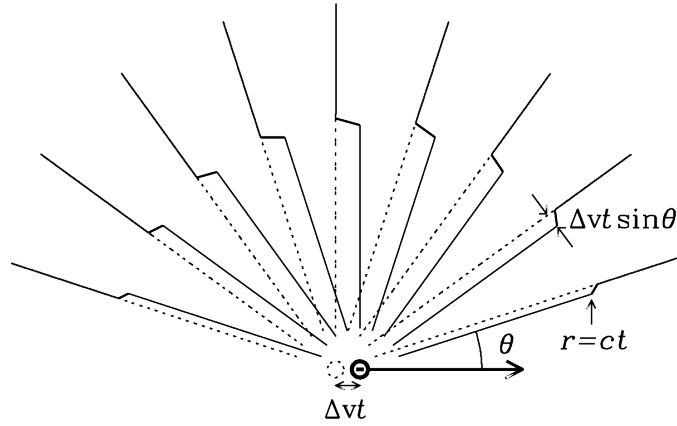## 2.7 Radiation from an Accelerated Charge

Fig. 8.— The electric field lines from an accelerated electron. The dotted circle shows the initial position of the electron, and the dotted lines are the radial lines of force emanating from that position. At time t after a small acceleration $\Delta v / \Delta t$, the electron position has moved by $\Delta v\, t$ and its lines of force have shifted transversely by $\Delta v\, t \sin \theta$.

Coulomb's law (Gaussian CGS form):

$$E_r = \frac{q}{r^2} \tag{34}$$

$$\frac{E_\perp}{E_r} = \frac{\Delta v\, t\, \sin \theta}{c \Delta t} \tag{35}$$

$$E_\perp = \frac{q \dot{v} \sin \theta}{r c^2} \tag{36}$$

$$\vec{S} = \frac{c}{4\pi} \vec{E} \times \vec{B} \qquad |\vec{S}| = \frac{c}{4\pi} E^2 = \left(\frac{q^2 \dot{v}^2}{4\pi c^3} \right) \frac{\sin^2 \theta}{r^2} \tag{37}$$

Larmor's equation: (classical, nonrelativistic)

$$P = \int_\mathrm{sphere} |\vec{S}|\, dA = \frac{2}{3} \frac{q^2 \dot{v}^2}{c^3} \tag{38}$$

Lecture 6:

Appendix A. Fourier Transforms

The Fourier transform of $f(x)$ is defined by

$$F(s) \equiv \int_{-\infty}^{\infty} f(x) \, e^{-2\pi i s x} \, dx \tag{39}$$

and

$$f(x) \equiv \int_{-\infty}^{\infty} F(s) \, e^{2\pi i s x} \, ds \;, \tag{40}$$

where the complex exponential

$$e^{i\phi} = \cos\phi + i\sin\phi \tag{41}$$

is a convenient way of dealing with sines and cosines (see *ERA* Appendix B3).

The symbol $\Leftrightarrow$ means "is the Fourier transform of"; e.g.,

$$F(s) \Leftrightarrow f(x) \;. \tag{42}$$

The discrete Fourier transform is defined by

$$X_k \equiv \sum_{j=0}^{N-1} x_j \, e^{-2\pi i j k / N} \tag{43}$$

and

$$x_j \equiv \frac{1}{N} \sum_{k=0}^{N-1} X_k \, e^{2\pi i j k / N} \;. \tag{44}$$

The sampling theorem says that any continuous function with a limited bandwidth $\Delta\nu$ can be reconstructed *exactly* from uniformly spaced samples separated in time by

$$\Delta t \le (2\Delta\nu)^{-1} \;. \tag{45}$$

The power spectrum of a continuous signal $f(x)$ is defined by $\overline{F(s)}F(s) = |F(s)|^2$. Rayleigh's theorem says the signal energies are the same in the time and frequency domains:

$$\int_{-\infty}^{\infty} |f(x)|^2 \, dx = \int_{-\infty}^{\infty} |F(s)|^2 \, ds \;. \tag{46}$$

Addition theorem:

$$f(x) + g(x) \Leftrightarrow F(s) + G(s). \tag{47}$$

Scaling theorem (a is any constant):

$$a f(x) \Leftrightarrow a F(s) \tag{48}$$

Shift theorem:
$$f(x - a) \Leftrightarrow e^{-2\pi i a s} F(s) \tag{49}$$

Similarity theorem:
$$f(ax) \Leftrightarrow \frac{F(s/a)}{|a|} \tag{50}$$

Modulation theorem:
$$f(x) \cos(2\pi\nu x) \Leftrightarrow \frac{1}{2} F(s - \nu) + \frac{1}{2} F(s + \nu) \tag{51}$$

Derivative theorem:
$$\frac{df}{dx} \Leftrightarrow i 2\pi s F(s) \tag{52}$$

The convolution $h(x)$ of the functions f and g is a linear functional defined by

$$h(x) = f * g \equiv \int_{-\infty}^{\infty} f(u) g(x - u) \, du \ . \tag{53}$$

Convolution theorem:
$$f * g \Leftrightarrow F \cdot G \tag{54}$$

Cross-correlation is represented by the pentagram symbol $\star$ and defined by

$$f \star g \equiv \int_{-\infty}^{\infty} f(u) g(u - x) \, du \ . \tag{55}$$

Cross-correlation theorem:
$$f \star g \Leftrightarrow \overline{F} \cdot G \tag{56}$$
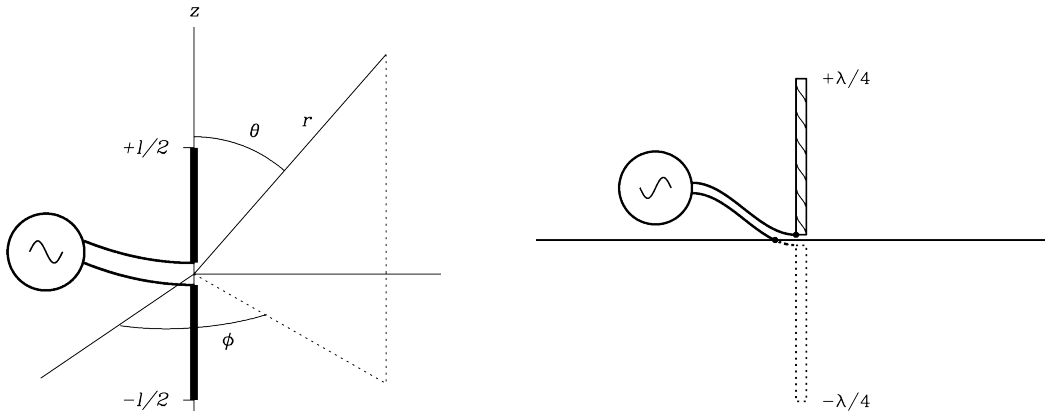
Autocorrelation is cross-correlation of a function with itself: $f \star f$. The autocorrelation theorem (a.k.a. Wiener–Khinchin theorem) states

$$f \star f \Leftrightarrow \overline{F} \cdot F = |F| \ , \tag{57}$$

so the Fourier transform of the autocorrelation function yields the signal power spectrum.

Lecture 7:

3.1 Antenna Fundamentals

An antenna is a passive device that converts electromagnetic radiation in space into electrical currents in conductors or vice versa, depending on whether it is being used for receiving or for transmitting, respectively. The simplest antenna is the short dipole of total length $l \ll \lambda$ driven by a current source $I = I_0 e^{-i\omega t}$. (See Appendix B.3 for a review of complex exponentials.) Electric current in a wire is defined as the charge flow rate

$$I \equiv \frac{dq}{dt} = \frac{dq}{dz}\frac{dz}{dt} = \frac{dq}{dz}v \ . \tag{58}$$

Using *ERA* Equation 2.136 in the derivation of Larmor's equation,

$$E_\perp = \frac{q\dot{v}\sin\theta}{rc^2} = \int_{z=-l/2}^{+l/2} \frac{dq}{dz}dz\frac{\dot{v}\sin\theta}{rc^2} = \frac{-i\omega\sin\theta}{rc^2}\int_{-l/2}^{+l/2} I\,dz \ . \tag{59}$$

For a linear current distribution tapering to $I = 0$ at the ends of the dipole,

$$I(z) \approx I_0 e^{-i\omega t}\left[1 - \frac{|z|}{(l/2)}\right] \quad \text{so} \quad \int_{-l/2}^{+l/2} I\,dz \approx \frac{I_0 l}{2}e^{-i\omega t} \tag{60}$$

and

$$E_\perp \approx \frac{-i\omega\sin\theta}{rc^2}\frac{I_0 l}{2}e^{-i\omega t} = \frac{-i\pi\sin\theta}{c}\frac{I_0 l}{\lambda}\frac{e^{-i\omega t}}{r} \ . \tag{61}$$

The time-averaged $[\langle\cos^2(\omega t)\rangle = 1/2]$ Poynting flux radiated

$$\langle S \rangle = \frac{c}{4\pi}\langle E_\perp^2\rangle\langle S\rangle = \frac{c}{4\pi}\left(\frac{1}{2}\right)\left(\frac{I_0 l}{\lambda}\frac{\pi}{c}\right)^2\frac{\sin^2\theta}{r^2} \tag{62}$$

has a doughnut-shaped $\sin^2\theta$ pattern, and the total time-averaged power radiated is

$$\langle P \rangle = \frac{\pi^2}{3c}\left(\frac{I_0 l}{\lambda}\right)^2 \ . \tag{63}$$

The power gain $G(\theta, \phi)$ of a transmitting antenna is defined as the power transmitted per unit solid angle in direction (θ, ϕ) relative to an isotropic antenna, which has the same gain in all directions. For a lossless antenna, energy conservation requires

$$\int_{\text{sphere}} G \, d\Omega = 4\pi \quad \text{so} \quad \langle G \rangle = 1 \ . \tag{64}$$

The effective area A_{e} of a receiving antenna is defined by

$$A_{\text{e}} \equiv \frac{2P_\nu}{S_\nu} \ , \tag{65}$$

where P_ν is the antenna response to an unpolarized point source of flux density S_ν.
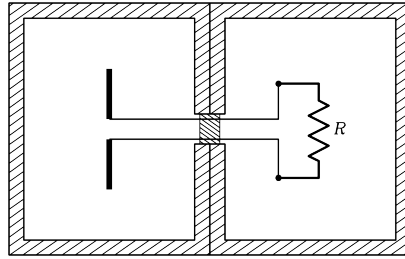
For *any* lossless antenna,

$$P_\nu = \frac{1}{2} \int_{4\pi} A_{\text{e}}(\theta, \phi) B_\nu \, d\Omega, \quad \langle A_{\text{e}} \rangle \equiv \frac{\int_{4\pi} A_{\text{e}} \, d\Omega}{\int_{4\pi} d\Omega} = \frac{1}{4\pi} \int_{4\pi} A_{\text{e}} \, d\Omega \ , \quad \text{so} \quad \langle A_{\text{e}} \rangle = \frac{\lambda^2}{4\pi} \ . \tag{66}$$

Reciprocity: An antenna can be treated either as a receiving device, gathering the incoming radiation field and conducting electrical signals to the output terminals, or as a transmitting system, launching electromagnetic waves outward. These two cases are equivalent because of time reversibility: the solutions of Maxwell's equations are valid when time is reversed.

Thus $G(\theta, \phi) \propto A_{\text{e}}(\theta, \phi)$. Using $\langle A_{\text{e}} \rangle = \lambda^2/(4\pi)$ and $\langle G \rangle = 1$,

$$A_{\text{e}}(\theta, \phi) = \frac{\lambda^2 G(\theta, \phi)}{4\pi} \ . \tag{67}$$

Antenna temperature is defined by

$$T_{\text{A}} \equiv \frac{P_\nu}{k} \ . \tag{68}$$

The antenna temperature produced by an unpolarized point source of flux density S_ν is

$$T_{\text{A}} = \frac{P_\nu}{k} = \frac{A_{\text{e}} S_\nu}{2k} \ . \tag{69}$$
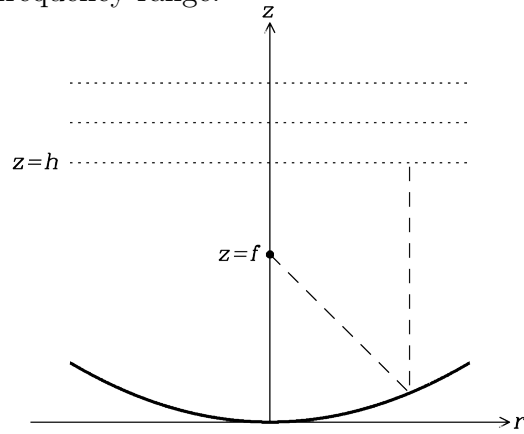
The main beam (MB) solid angle is defined by

$$\Omega_{\text{MB}} \equiv \frac{1}{G_0} \int_{\text{MB}} G(\theta, \phi) \, d\Omega \ . \tag{70}$$

Lecture 8:

3.2 Reflector Antennas

Reflector antennas have effective areas approaching their geometric areas, are electrically simple, and cover a wide frequency range.

$$\text{Equation of a paraboloid}: \quad z = \frac{r^2}{4f} \tag{71}$$

For best performance, targets must not be closer than the far-field distance

$$R_{\text{ff}} \approx \frac{2D^2}{\lambda} \ . \tag{72}$$

The aperture of a reflector antenna is the opening through which all rays pass.
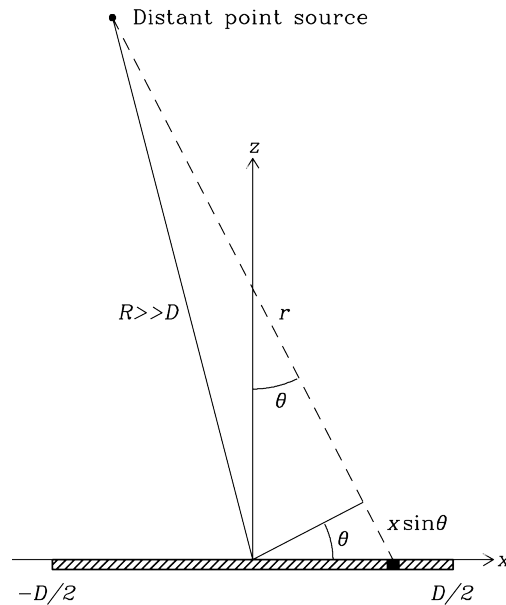
The beam pattern of an antenna system is its power gain as a function of direction. The electric field pattern is the square root of the beam power pattern.

Huygen's principle: The aperture can be treated as a collection of small elements acting individually. The electric field contributed by the element from x to $x + dx$ is

$$df \propto g(x)\frac{\exp(-i2\pi r(x)/\lambda)}{r(x)}dx \ . \tag{73}$$

The Fraunhofer approximation in the far field is

$$r \approx R + x\sin\theta = R + xl \quad \text{where} \quad l \equiv \sin\theta \ . \tag{74}$$

$$df \propto g(x)\exp(-i2\pi xl/\lambda)dx \ . \tag{75}$$

Define $u \equiv x/\lambda$ and integrate to get the aperture field pattern

$$f(l) = \int_{\text{aperture}} g(u)e^{-i2\pi lu}du \ , \tag{76}$$

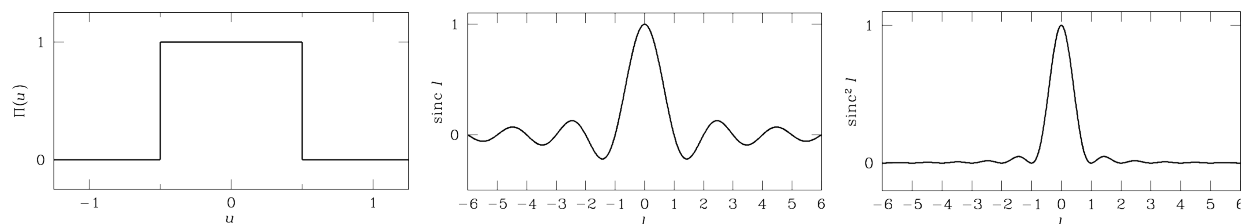which is the Fourier transform of the field illumination $g(u)$.

Example: Uniform illumination of a one-dimensional aperture of width D:

$$g(u) = \text{ constant}, \qquad -\frac{D}{2\lambda} < u < +\frac{D}{2\lambda} \tag{77}$$

$$f(l) = \int_{-1/2}^{+1/2} e^{-i2\pi lu}du = \frac{e^{-i2\pi lu}}{-i2\pi l}\bigg|_{-1/2}^{+1/2} = \frac{e^{-i\pi l} - e^{i\pi l}}{-i2\pi l} = \frac{\sin(\pi l)}{(\pi l)} \equiv \text{sinc}(l) \tag{78}$$

In the limit $\theta \ll 1$ radian, $l = \sin\theta \approx \theta$ and the field and power patterns are

$$f(\theta) = \frac{D}{\lambda}\text{ sinc}\left(\frac{\theta D}{\lambda}\right) \qquad \text{and} \qquad P(\theta) = f^2(\theta) = \left(\frac{D}{\lambda}\right)^2 \text{sinc}^2\left(\frac{\theta D}{\lambda}\right) \ . \tag{79}$$

Resolving power = diffraction-limited half-power beamwidth: $\theta_{\text{HPBW}} \approx 0.89\lambda/D$.

Example: Cosine-tapered illumination is more practical, yields lower sidelobes, slightly lower aperture efficiency, and slightly larger beamwidth $\theta_{\text{HPBW}} \approx 1.2\lambda/D$.
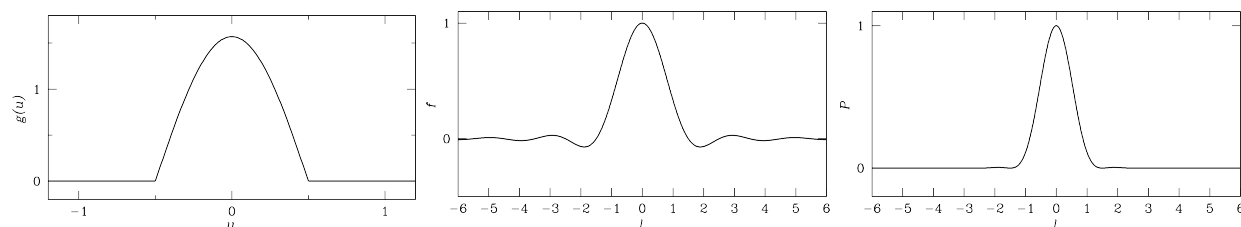
Lecture 9:

3.3 Two-Dimensional Aperture Antennas

The electric field pattern of a two-dimensional aperture is the two-dimensional Fourier transform of the aperture field illumination:

$$f(l, m) \propto \int_{-\infty}^{\infty} \int_{-\infty}^{\infty} g(u, v) e^{-i2\pi(lu+mv)} du \, dv, \tag{80}$$

where m is the y-axis analog of l on the x-axis and $v \equiv y/\lambda$.

The field and power patterns of a uniformly illuminated rectangular aperture are:

$$f(l, m) \propto \mathrm{sinc}\left(\frac{lD_x}{\lambda}\right) \mathrm{sinc}\left(\frac{mD_y}{\lambda}\right) \quad \text{and} \quad P_{\mathrm{n}}(l, m) = \mathrm{sinc}^2\left(\frac{lD_x}{\lambda}\right) \mathrm{sinc}^2\left(\frac{mD_y}{\lambda}\right) . \tag{81}$$

The absolute power gain G in any direction can be calculated from the relative power pattern by invoking energy conservation:

$$\int G \, d\Omega = 4\pi = G_0 \int_{-1}^{+1} \int_{-1}^{+1} P_{\mathrm{n}}(l, m) dl \, dm \; ; \tag{82}$$

it is

$$G = \left(\frac{4\pi D_x D_y}{\lambda^2}\right) \mathrm{sinc}^2\left(\frac{lD_x}{\lambda}\right) \mathrm{sinc}^2\left(\frac{mD_y}{\lambda}\right) \approx \left(\frac{4\pi D_x D_y}{\lambda^2}\right) \mathrm{sinc}^2\left(\frac{\theta_x D_x}{\lambda}\right) \mathrm{sinc}^2\left(\frac{\theta_y D_y}{\lambda}\right) \tag{83}$$

Aperture efficiency η_{A} is defined as the ratio of the on-axis effective area $A_0 = \lambda^2 G_0/(4\pi)$ to the geometric area:

$$\eta_{\mathrm{A}} \equiv \frac{A_0}{A_{\mathrm{geom}}} . \tag{84}$$

It is $\eta_{\mathrm{A}} = 1$ for a uniformly illuminated aperture and $\eta_{\mathrm{A}} < 1$ otherwise.

Gaussian beams: Most radio telescopes have nearly Gaussian beams

$$\Omega_{\mathrm{A}} = \int_{\theta=0}^{\infty} \int_{\phi=0}^{2\pi} \exp\left[-4\ln 2\left(\frac{\theta}{\theta_{\mathrm{HPBW}}}\right)^2\right] \theta \, d\phi \, d\theta , \tag{85}$$

where the half power beam width (HPBW) = full width between half-maximum (FWHM) points. The Gaussian beam solid angle is

$$\Omega_{\mathrm{A}} = \int_{\theta=0}^{\infty} \int_{\phi=0}^{2\pi} \exp\left[-4\ln 2\left(\frac{\theta}{\theta_{\mathrm{HPBW}}}\right)^2\right] \theta \, d\phi \, d\theta = \left(\frac{\pi}{4\ln 2}\right) \theta_{\mathrm{HPBW}}^2 \approx 1.133 \, \theta_{\mathrm{HPBW}}^2 . \tag{86}$$

Reflector surface accuracy: Ruze equation for reflector surface efficiency:

$$\eta_{\mathrm{s}} = \exp\left[-\left(\frac{4\pi\sigma}{\lambda}\right)^2\right] \tag{87}$$

Good performance requires $\sigma \lesssim \lambda_{\min}/16$. Similarly, the rms pointing errors in each coordinate should be no larger than $\sigma_1 \sim \theta_{\mathrm{HPBW}}/10$. Differential solar heating and wind gusts are major contributors to pointing errors.

3.4 Waveguides

Waveguides are low-loss shielded "pipes" used to transport electromagnetic waves between antennas and receivers or between sections of a receiver. At the conducting walls, the parallel component of any electric field inside the waveguide must be zero, so waves travel down the waveguide with group velocity

$$v_{\mathrm{g}} = c \sin \alpha = c (1 - \cos^2 \alpha)^{1/2} = c \left[1 - \left(\frac{\nu_{\mathrm{c}}}{\nu} \right)^2 \right]^{1/2} , \tag{88}$$

and the cutoff wavelength ($\cos \alpha = 1$ so $v_{\mathrm{g}} = 0$) is $\lambda_{\mathrm{c}} = 2a$. To suppress higher-order modes, waveguides are rarely used at frequencies $\nu > 2\nu_{\mathrm{c}}$. Each feed and receiver on a radio telescope covers only one waveguide band, so several feeds and receivers are needed to span the much wider useful frequency range of the telescope itself.
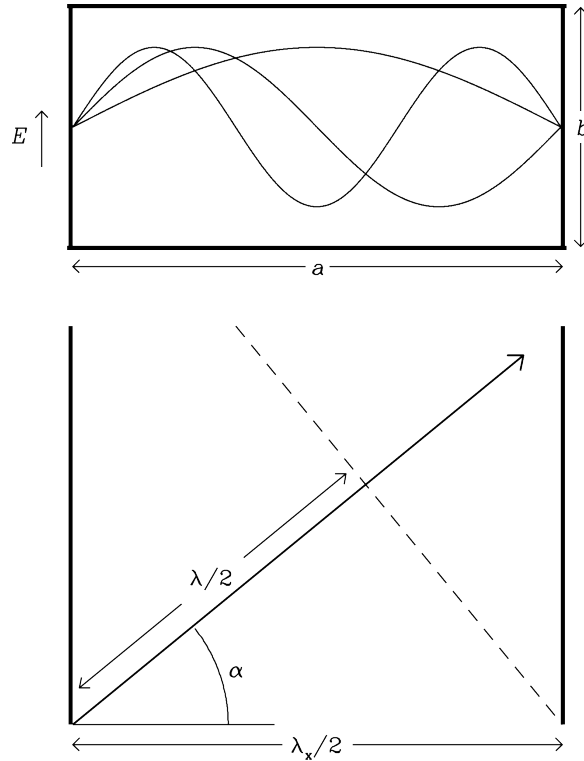
Lecture 10:

3.5 Radio Telescopes

Dipole arrays are practical only at wavelengths $\lambda \gtrsim 1$ m

Waveguide horns have unblocked apertures and pick up very little ground radiation, so they can measure absolute sky temperatures (e.g., the Bell Labs horn that detected the 2.73 K CMB at $\nu \approx 4$ GHz). They also have nearly uniform aperture illumination, so their absolute collecting areas can be calculated accurately and they can be used to make absolute flux-density measurements of strong sources.

Large steerable parabolic dishes can have equatorial mounts (e.g., the 140-foot telescope in Green Bank) but most have mechanically simpler alt-az mounts that turn on horizontal azimuth tracks and tip in "altitude" (elevation angle above the horizon).

Small prime-focus feeds are normally used at wavelengths $\lambda \gtrsim 0.3$ m ($\nu \lesssim 1$ GHz). Magnifying subreflectors requiring larger feeds are favored at shorter wavelengths because:

1. They multiply the effective f/D ratio; values of $f/D \sim 2$ are typical. This greatly increases the size of the focal ellipsoid. Multiple feeds can be located within the focal ellipsoid to produce multiple simultaneous beams for faster imaging.

2. The subreflector is many wavelengths in diameter so the illumination taper can be tailored to optimize the tradeoff between high aperture efficiency and low sidelobes.

3. Receivers can be located near the vertex, where they are easier to access.

4. Feed spillover radiation is directed toward the cold sky instead of the warm ground.

5. The subreflector can rapidly nutate (switch the beam between two adjacent positions on the sky) to differentiate (cancel out) slow receiver and atmospheric noise drifts.

6. The subreflector can be tilted to select any of several feeds at the secondary focus.
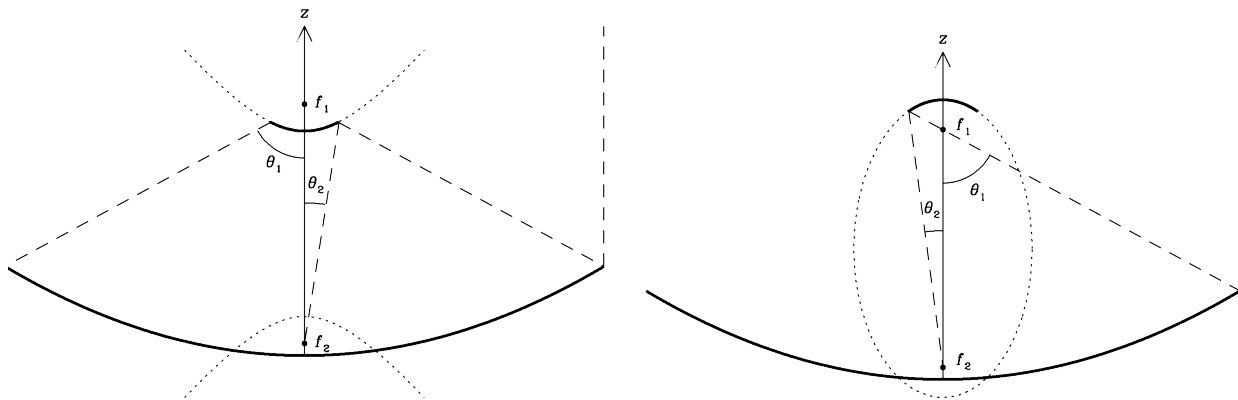
Homology telescopes have backup structures that deform to maintain a parabolic surface while tilting; only the focus shifts, and the feed/subreflector can track the shifting focus.

The 305 m (1000 foot) Arecibo telescope has a fixed spherical reflector and can be steered up to 20° from the zenith by moving the feeds. Spherical aberrations are corrected by waveguide line feeds or shaped subreflectors.

The 100 m Green Bank Telescope (GBT) is an offset section of a 208 m "parent" paraboloid so its aperture is unblocked. The offset feed arm can be large because it is not blocking
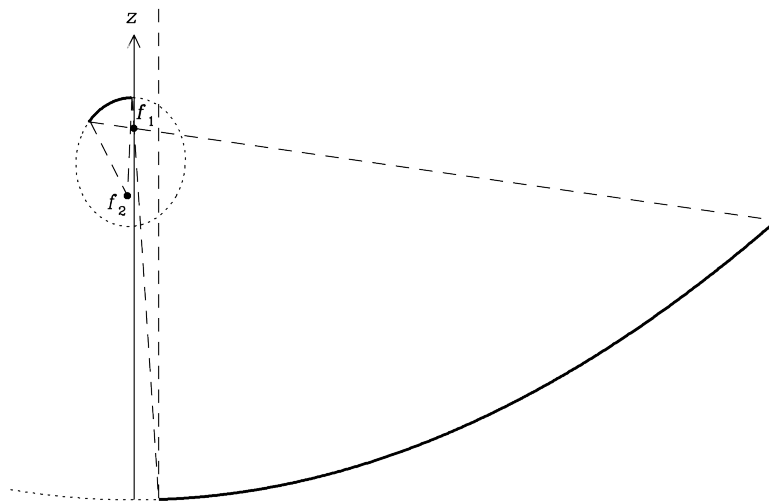
the aperture. It is strong enough to hold the subreflector plus a large receiver cabin at the Gregorian secondary focus. The secondary focus is not far below the prime focus, so the subreflector subtends a large solid angle as seen by the Gregorian feeds, which are not large. The GBT is homologous and also has an active surface with ≈ 2000 panels that are adjusted in real time to compensate for surface errors. In good conditions, the GBT surface error is only $\sigma \approx 0.21$ mm and the GBT is efficient up to $\nu \sim 100$ GHz.

Lecture 11:

3.6 Radiometers

A radiometer is a receiver that measures the average power of noise coming from a radio telescope in some frequency range $\Delta\nu$. A square-law detector in the radiometer squares the noise voltage to produce an output noise voltage proportional to the input noise power.
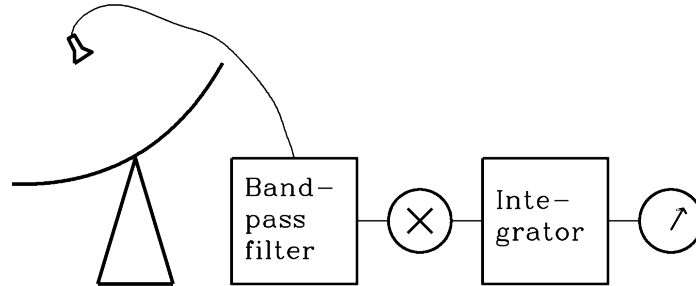
The noise power of most astronomical sources is stationary (steady) on timescales $\tau \gg \nu^{-1}$. The sampling theorem says that any function with bandwidth $\Delta\nu$ and duration τ can be represented by $2\Delta\nu\,\tau$ independent samples spaced in time by $(2\Delta\nu)^{-1}$. By averaging a large number $N = (2\Delta\nu\,\tau)$ samples, an ideal radiometer can determine the average noise power with a fractional rms error as small as $(N/2)^{-1/2} = (\Delta\nu\,\tau)^{-1/2} \ll 1$.

The noise temperature of any noiselike source is defined by

$$T_{\mathrm{N}} \equiv \frac{P_\nu}{k} \; . \tag{89}$$

The system noise temperature is the sum of all noise contributions

$$T_{\mathrm{s}} = T_{\mathrm{cmb}} + T_{\mathrm{rsb}} + \Delta T_{\mathrm{source}} + [1 - \exp(-\tau_{\mathrm{A}})]T_{\mathrm{atm}} + T_{\mathrm{spill}} + T_{\mathrm{r}} + \cdots, \tag{90}$$

where $T_{\mathrm{cmb}} \approx 2.73$ K is the cosmic microwave background, T_{rb} is the average sky brightness produced by radio sources, $\Delta T_{\mathrm{source}}$ is from the source being observed, $[1 - \exp(-\tau_{\mathrm{A}})]T_{\mathrm{atm}}$ is atmospheric emission in the telescope beam, T_{spill} is spillover pickup, T_{r} is the radiometer noise temperature, and ... represents other noise sources such as ohmic losses.

Ideal total-power radiometer equation for rms output noise fluctuations:

$$\sigma_T \approx \frac{T_{\mathrm{s}}}{\sqrt{\Delta\nu\,\tau}} \tag{91}$$

Fractional gain fluctuations $\Delta G/G$ in practical total-power radiometers increase the noise to

$$\sigma_T \approx T_{\mathrm{s}}\left[\frac{1}{\Delta\nu\,\tau} + \left(\frac{\Delta G}{G}\right)^2\right]^{1/2} \; . \tag{92}$$

Dicke radiometer:
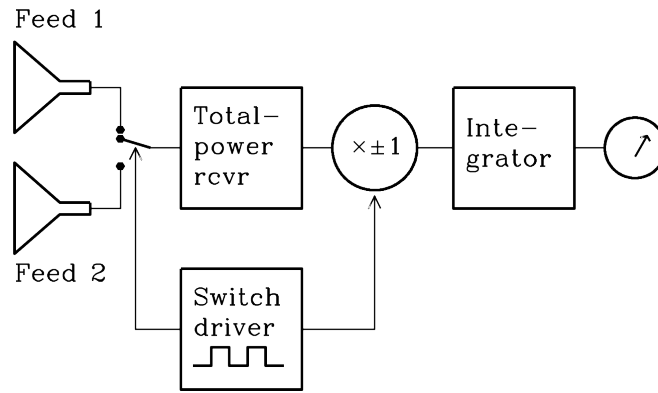
$$\sigma_T = \frac{2T_{\mathrm{s}}}{\sqrt{\Delta\nu\,\tau}} \tag{93}$$

Superheterodyne receivers:

Confusion: sky brightness fluctuations from numerous faint sources in every telescope beam.

Lecture 12:

3.7 Interferometers I

A single dish of diameter D has diffraction-limited resolution $\theta \approx \lambda/D$, collecting area $\lesssim \pi D^2/4$, a field of view containing at most a few beams, and must have mechanical pointing errors $\sigma \lesssim \theta/10$. Fully steerable dishes larger than $D \sim 100$ m are impractical.

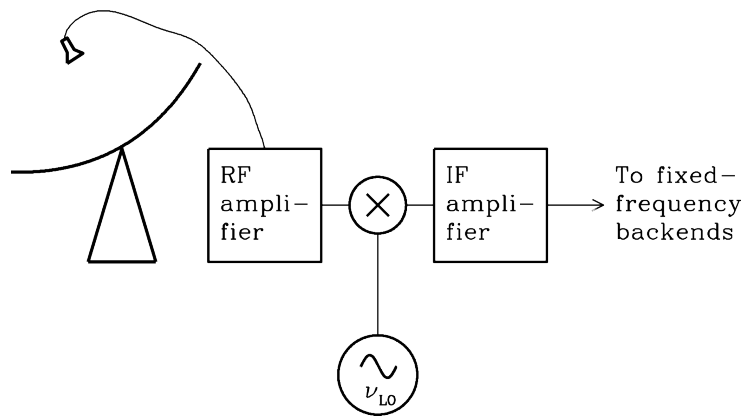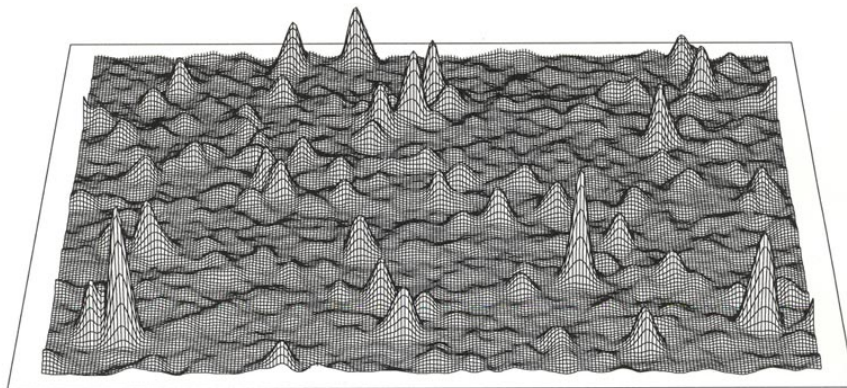A interferometric array of N relatively small dishes has resolution $\theta \approx \lambda/b$, where $b \gg D$ is the maximum baseline separating the dishes, collecting area $\lesssim N\pi D^2/4$, a field of view covering $\theta^2 \sim (\lambda/D)^2$ containing $\sim (b/D)^2 \gg 1$ resolution elements, and can measure positions with uniquely high accuracy $\sigma \ll 1''$ by using clocks instead of rulers. Interferometers are less vulnerable to fluctuations in atmospheric emission and receiver gain, radio frequency interference, and pointing shifts caused by atmospheric refraction. Interferometers do not respond to smooth emission extended over angles $\gg \lambda/D$, and very large $(b \gg D)$ interferometers have poor surface-brightness sensitivity. Sensitive arrays with $N \gg 1$ elements require coherent amplifiers, so they are limited to radio frequencies by quantum noise.
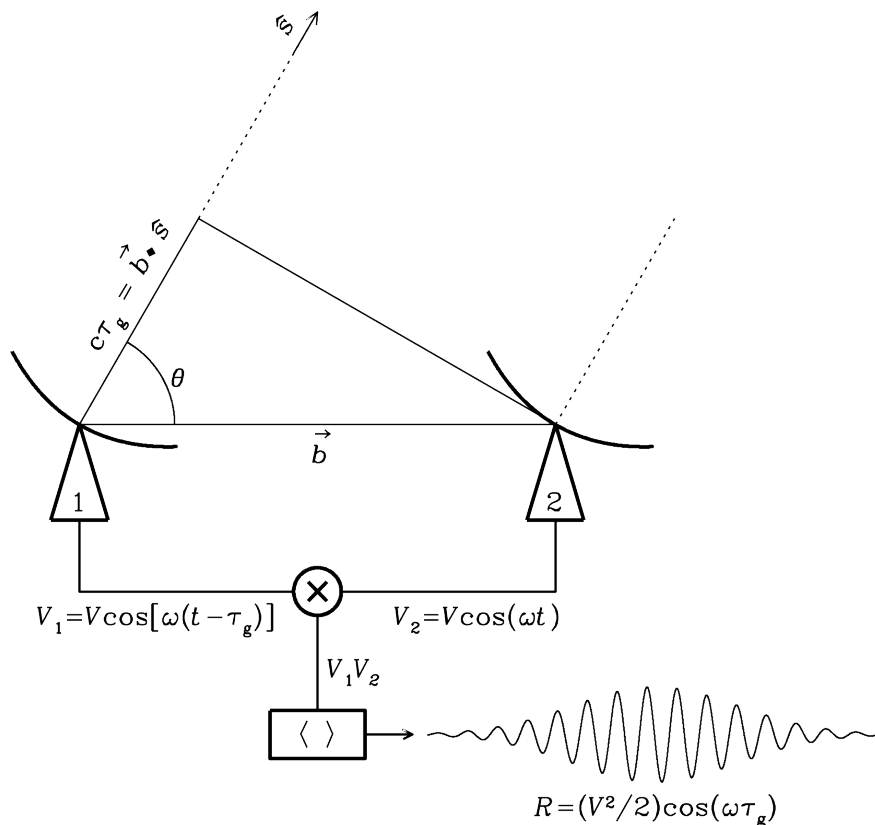

Fig. 9.— A two-element quasi-monochromatic multiplying interferometer with baseline $\vec{b}$ observing a source in direction $\hat{s}$ responds to the Fourier component of sky brightness with angular period $\lambda/(b\sin\theta)$. The broad Gaussian envelope of the sinusoidal output is the primary attenuation pattern of the individual dishes.

An array with N elements contains $N(N-1)/2$ two-element interferometers. As N grows, its synthesized or "dirty" beam becomes nearly Gaussian: However, the sum of sinusoids
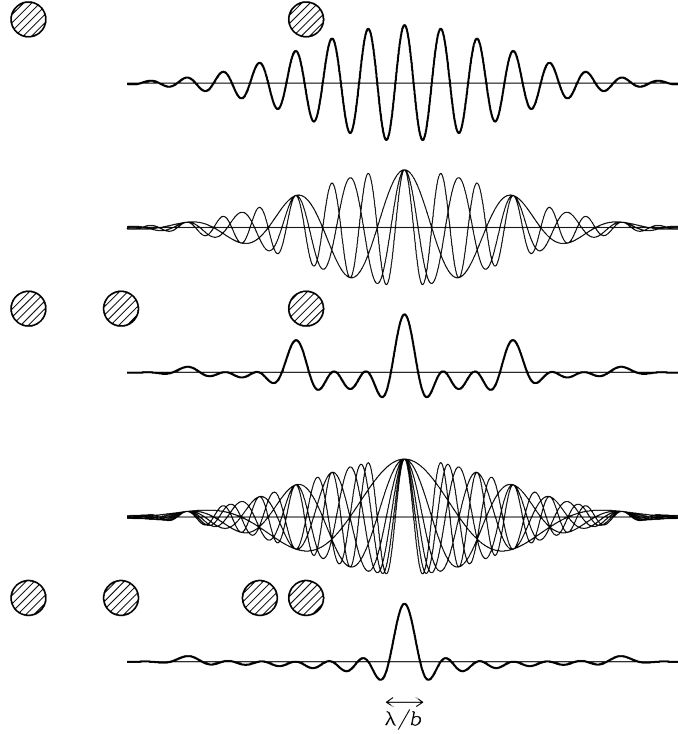
has zero average, so there is a broad and shallow negative "bowl" under the Gaussian main lobe.

The cosine correlator shown in Figure 9 responds only to even brightness distributions

$$R_{\rm c} = \int I(\hat{s}) \cos(2\pi \vec{b} \cdot \hat{s}/\lambda)\, d\Omega \tag{94}$$

so it must be complemented by an odd sine correlator with response

$$R_{\rm s} = \int I(\hat{s}) \sin(2\pi \vec{b} \cdot \hat{s}/\lambda)\, d\Omega \tag{95}$$

to image all brightness distributions. Such a complex correlator yields a complex visibility

$$\mathcal{V} \equiv R_{\rm c} - i R_{\rm s} = A e^{-i\phi} = \int I(\hat{s}) \exp(-i2\pi \vec{b} \cdot \hat{s}/\lambda)\, d\Omega \ , \tag{96}$$

where $A = (R_{\rm c}^2 + R_{\rm s}^2)^{1/2}$ is the visibility amplitude and $\phi = \tan^{-1}(R_{\rm s}/R_{\rm c})$ is the phase.

Compensating for the geometric delay $\tau_0 = \vec{b} \cdot \vec{s_0}/c$ in direction s_0 allows imaging at resolution $\theta_{\rm s}$ out to radius $\Delta\theta$ with finite bandwidth $\Delta\nu$ and finite sampling time Δt given by

$$\frac{\Delta\theta}{\theta_{\rm s}} \ll \frac{\nu}{\Delta\nu} \qquad \text{and} \qquad \frac{2\pi\Delta t}{P} \approx \frac{\Delta t}{1.37 \times 10^4\ {\rm s}} \ll \frac{\theta_{\rm s}}{\Delta\theta} \ . \tag{97}$$

Lecture 13:

3.7 Interferometers II

The Earth's rotation varies the projected baseline coverage of an interferometer whose elements are fixed on the ground. All baselines of an east–west interferometer remain in a single plane perpendicular to the Earth's north–south rotation axis as the Earth turns daily, so the brightness distribution of a source is simply the two-dimensional Fourier transform of the measured visibilities.
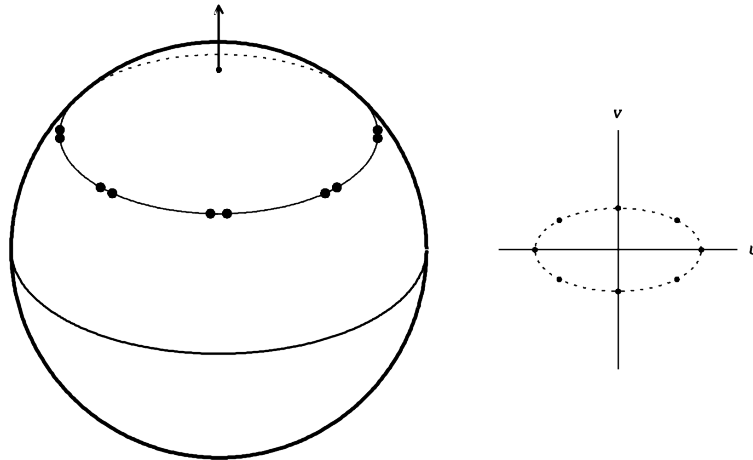
Fig. 10.— Viewed from a distant radio source at declination $\delta = +30°$ the antennas of a two-element east–west interferometer at latitude $+40°$ are shown as they would appear at hour angles -6^{h}, -3^{h}, 0^{h}, $+3^{\mathrm{h}}$, and $+6^{\mathrm{h}}$. The projected baseline traces an ellipse in the (u, v) plane. The v-axis of the ellipse is smaller by a factor $\sin \delta$ than the u-axis.

If the baselines are not confined to an east–west line, Earth rotation causes them to fill a three-dimensional volume: The w axis points to the source in direction s_0. The direction
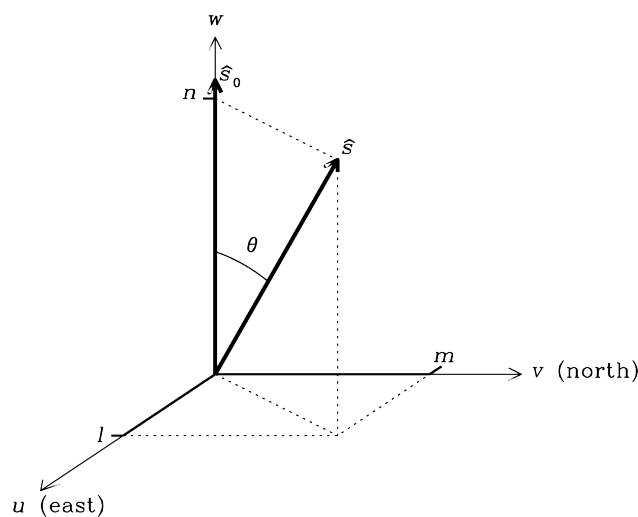
cosines l, m, and $n = \cos\theta = (1 - l^2 - m^2)^{1/2}$, so

$$d\Omega = \frac{dl\,dm}{(1 - l^2 - m^2)^{1/2}} \tag{98}$$

and

$$\mathcal{V}(u, v, w) = \int\int \frac{I_\nu(l, m)}{(1 - l^2 - m^2)^{1/2}} \exp[-i2\pi(ul + vm + wn)]dl\,dm \ . \tag{99}$$

In directions near $\hat{s}_0$, $w\theta^2 \ll 1$ and $\theta \ll s^{-1/2} \approx (\lambda/b)^{1/2}$, so

$$\mathcal{V}\exp(i2\pi w) = \int\int \frac{I_\nu(l, m)}{(1 - l^2 - m^2)^{1/2}} \exp[-i2\pi(ul + vm)]dl\,dm \ . \tag{100}$$

A field wider than $\theta \ll w^{-1/2}$ can be imaged with two-dimensional Fourier transforms by breaking it up into smaller facets, much like a fly's eye, and later merging the facets.

The effective collecting area A_e of a two-element interferometer equals the effective collecting area of each element. The correlator output noise is $2^{1/2}$ lower than the square-law detector noise of each antenna. The rms noise per polarization for a two-element interferometer is

$$\sigma_S = \frac{2^{1/2}kT_\mathrm{s}}{A_\mathrm{e}(\Delta\nu\,\tau)^{1/2}} \ . \tag{101}$$

An array of N antennas contains $N(N - 1)/2$ independent two-element interferometers, so its rms noise per polarization is

$$\sigma_S = \frac{2kT_\mathrm{s}}{A_\mathrm{e}[N(N - 1)\Delta\nu\,\tau]^{1/2}} \ . \tag{102}$$

In the limit $N \gg 1$, $[N(N - 1)]^{1/2} \to N$ and the effective area of an interferometer approaches NA_e. Quantized digital correlators reduce the sensitivity (increase the noise) by their correlator efficiency. For example, a three-level correlator has $\eta_\mathrm{c} \approx 0.89$.

The brightness sensitivity of an interferometer with the same point-source sensitivity as a single dish is lower by a factor $\approx (D/b)^2$ approximately equal to the area covering factor of the array, because the synthesized beam area Ω_A is lower by this factor. In the Rayleigh-Jeans limit

$$\sigma_T = \left(\frac{\sigma_S}{\Omega_\mathrm{A}}\right)\frac{\lambda^2}{2k} \ . \tag{103}$$

If the interferometer image is restored with a Gaussian beam,

$$\Omega_\mathrm{A} = \frac{\pi\theta_\mathrm{HPBW}^2}{4\ln 2} \tag{104}$$

and

$$\sigma_T = \left(\frac{2\ln 2\,c^2}{\pi k\nu^2}\right)\frac{\sigma_S}{\theta_\mathrm{HPBW}^2} \ . \tag{105}$$

Lecture 14:

4.1 Free–Free Radiation I

Thermal emission is produced by a source whose emitting particles are in local thermodynamic equilibrium; e.g., radiating electrons have a Maxwellian velocity distribution (Appendix B.8). Free-free radiation is Larmor radiation from free electrons accelerated by electrostatic scattering off ions:

$$|\dot{v}| = \frac{F}{m_{\mathrm{e}}} = \frac{Ze^2}{m_{\mathrm{e}}r^2} \; , \tag{106}$$

where $m_{\mathrm{e}} \approx 9.1 \times 10^{-28}$ g is the electron mass and r is the distance between the electron and the much heavier ion with Z electrons removed.
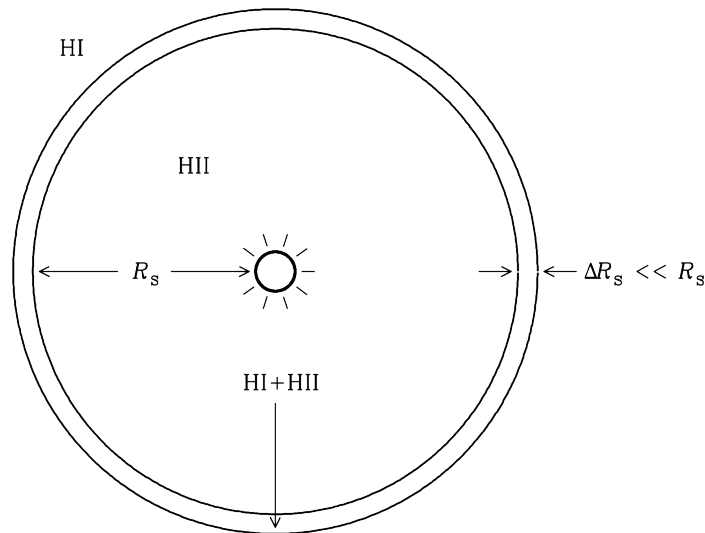
Fig. 11.— A Strömgren sphere of ionized hydrogen (Hii) with Strömgren radius R_{S} inside a thin shell of partially ionized hydrogen (Hi + Hii) surrounded by neutral hydrogen (Hi).

Radio radiation from a single electron-ion interaction: The distance of closest approach b
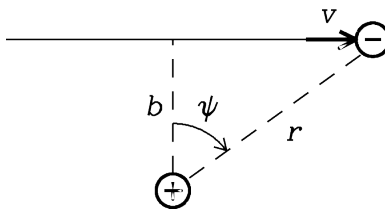
is called the impact parameter and the interval $\tau = b/v$ is called the collision time. The Larmor radiation power is

$$P = \frac{2}{3}\frac{e^2\dot{v}_{\perp}^2}{c^3} = \frac{2e^2}{3c^3}\frac{Z^2e^4}{m_{\mathrm{e}}^2}\left(\frac{\cos^3\psi}{b^2}\right)^2 \tag{107}$$

and the total energy W emitted during the interaction of duration

$$dt = \frac{b}{v} \frac{d\psi}{\cos^2 \psi} \tag{108}$$

is

$$W = \int_{-\infty}^{\infty} P \, dt = \frac{2}{3} \frac{Z^2 e^6}{c^3 m_e^2 b^4} \int_{-\pi/2}^{\pi/2} \frac{b \cos^6 \psi}{v \cos^2 \psi} d\psi = \frac{\pi Z^2 e^6}{4c^3 m_e^2} \left(\frac{1}{b^3 v} \right). \tag{109}$$

In a $T \sim 10^4$ K H$_{\text{II}}$ region, $v \approx 7 \times 10^7$ cm s^{-1} and the minimum impact parameter is $b_{\text{min}} \sim 10^{-7}$ cm, so $\nu_{\text{max}} \approx 10^{14}$ Hz, much higher than radio frequencies. In the approximation that the power spectrum is flat out to $\nu = \nu_{\text{max}}$ and zero at higher frequencies, the average energy *per unit frequency* emitted during a single interaction is approximately

$$W_\nu \approx \frac{W}{\nu_{\text{max}}} = \left(\frac{\pi Z^2 e^6}{4c^3 m_e^2 b^3 v} \right) \left(\frac{2\pi b}{v} \right) \approx \frac{\pi^2}{2} \frac{Z^2 e^6}{c^3 m_e^2} \left(\frac{1}{b^2 v^2} \right). \tag{110}$$

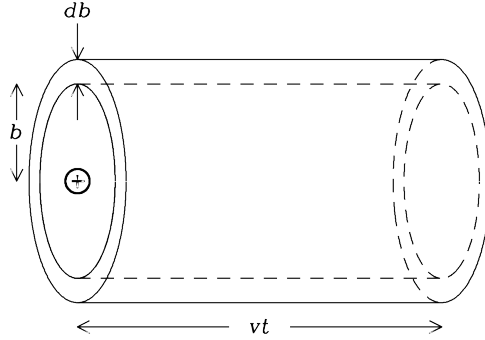Radio radiation from an H$_{\text{II}}$ region: The number of electrons with speeds v to $v + dv$ passing

by a stationary ion and having impact parameters in the range b to $b + db$ during the time interval t equals the number of electrons with speeds v to $v + dv$ in the cylindrical shell:

$$n_e \, (2\pi b \, db) \, v \, f(v) \, dv \, , \tag{111}$$

where $f(v)$ is the normalized ($\int f(v) dv = 1$) speed distribution of the electrons. The number $\dot{n}_c(v, b)$ of such collisions per unit volume per unit time is

$$\dot{n}_c(v, b) = (2\pi b) v f(v) \, n_e n_i \, . \tag{112}$$

The spectral power at frequency ν emitted isotropically per unit volume is $4\pi j_\nu$, where j_ν is the emission coefficient. Thus

$$4\pi j_\nu = \int_{b=0}^{\infty} \int_{v=0}^{\infty} W_\nu(v, b) \dot{n}_c(v, b) dv \, db = \frac{\pi^3 Z^2 e^6 n_e n_i}{c^3 m_e^2} \int_{v=0}^{\infty} \frac{f(v)}{v} dv \int_{b_{\text{min}}}^{b_{\text{max}}} \frac{db}{b} \, . \tag{113}$$

where the finite limits b_{min} and b_{max} are needed to avoid divergence.

Lecture 15:

4.1 Free–Free Radiation II

For the nonrelativistic Maxwellian velocity distribution (*ERA* Appendix B.8)

$$f(v) = \frac{4v^2}{\sqrt{\pi}}\left(\frac{m_e}{2kT}\right)^{3/2}\exp\left(-\frac{m_e v^2}{2kT}\right) \quad \text{so} \tag{114}$$

$$\int_{v=0}^{\infty}\frac{f(v)}{v}dv = \frac{4}{\sqrt{\pi}}\left(\frac{m_e}{2kT}\right)^{3/2}\int_{v=0}^{\infty}v\exp\left(-\frac{m_e v^2}{2kT}\right)dv = \left(\frac{2m_e}{\pi kT}\right)^{1/2} \tag{115}$$

and the free-free emission coefficient is

$$j_\nu = \frac{\pi^2 Z^2 e^6 n_e n_i}{4c^3 m_e^2}\left(\frac{2m_e}{\pi kT}\right)^{1/2}\ln\left(\frac{b_{max}}{b_{min}}\right). \tag{116}$$

The maximum possible momentum transfer $m_e\Delta v$ during the free–free interaction is twice the initial momentum $m_e v$ of the electron, so the impact parameter of a free–free interaction cannot be smaller than

$$b_{min} \approx \frac{Ze^2}{m_e v^2} \approx 5.6 \times 10^{-8} \text{ cm} \tag{117}$$

if $T \approx 10^4$ K. b_{max} is he largest value of b that can generate a significant amount of power at some relevant radio frequency ν. Recall that the pulse power per unit bandwidth is small above angular frequency $\omega \approx v/b$ so

$$b_{max} \approx \frac{v}{\omega} = \frac{v}{2\pi\nu} \approx 1.1 \times 10^{-2} \text{ cm} \quad \text{if } T \approx 10^4 \text{ K}. \tag{118}$$

In LTE at temperature T, Kirchhoff's law gives the absorption coefficient

$$\kappa = \frac{j_\nu}{B_\nu(T)} \approx \frac{j_\nu c^2}{2kT\nu^2} = \frac{1}{\nu^2 T^{3/2}}\left[\frac{Z^2 e^6}{c}n_e n_i\frac{1}{\sqrt{2\pi(m_e k)^3}}\right]\frac{\pi^2}{4}\ln\left(\frac{b_{max}}{b_{min}}\right). \tag{119}$$

The limit $b_{max} \propto \nu^{-1}$ so a good numerical approximation is $\kappa \propto \nu^{-2.1}$ and

$$\tau = -\int_{los}\kappa\,ds \propto \int\frac{n_e n_i}{\nu^{2.1}T^{3/2}}ds \approx \int\frac{n_e^2}{\nu^{2.1}T^{3/2}}ds. \tag{120}$$

The emission measure (EM) of an H<small>II</small> region is defined by the integral of n_e^2 along the line of sight expressed in astronomically convenient units:

$$\frac{\text{EM}}{\text{pc cm}^{-6}} \equiv \int_{los}\left(\frac{n_e}{\text{cm}^{-3}}\right)^2 d\left(\frac{s}{\text{pc}}\right), \tag{121}$$

and a simple but good approximation for the free-free opacity is

$$\tau \approx 3.28 \times 10^{-7}\left(\frac{T}{10^4 \text{ K}}\right)^{-1.35}\left(\frac{\nu}{\text{GHz}}\right)^{-2.1}\left(\frac{\text{EM}}{\text{pc cm}^{-6}}\right). \tag{122}$$
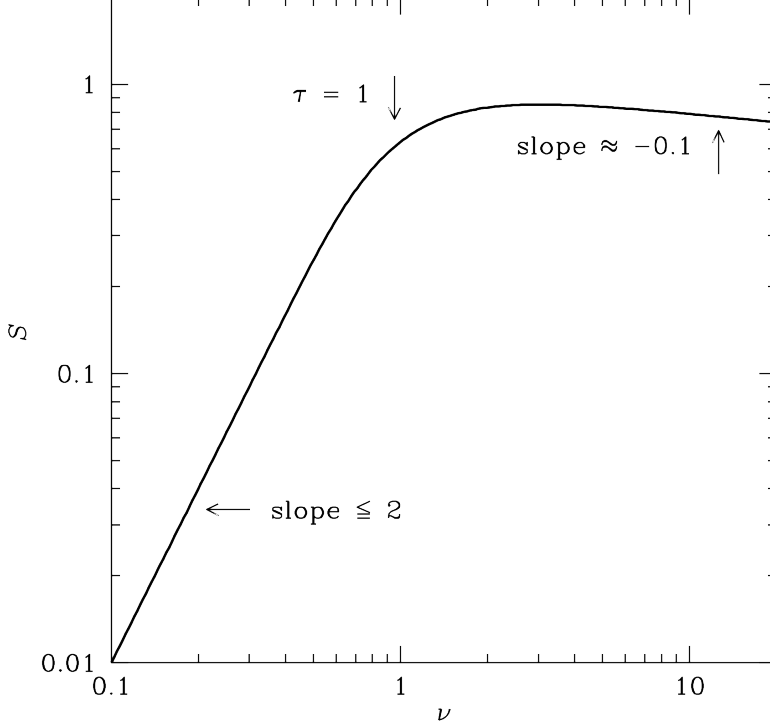
Fig. 12.— The radio spectrum of an HII region is a blackbody at low frequencies, with spectral index $\alpha = +2$ for a uniform cylinder and < 2 otherwise. At some frequency ν the optical depth $\tau = 1$, and at much higher frequencies $\alpha \approx -0.1$ because the opacity coefficient $\kappa(\nu) \propto \nu^{-2.1}$. The source brightness at low frequencies equals the electron temperature, and the brightness at high frequencies is proportional to the emission measure.

The optical depth τ and electron temperature T yield the brightness temperature

$$T_{\mathrm{b}} = T(1 - e^{-\tau}) \tag{123}$$

of free–free emission. The line-of-sight structure of an HII region is not normally known, so it is common to approximate the geometry of an HII region by a circular cylinder whose axis lies along the line of sight, and whose axis length equals its diameter. If the temperature and density are constant throughout this volume and the HII region distance is known, it is easy to estimate the electron density, temperature, emission measure, and production rate Q_{H} of ionizing photons from the observed radio spectrum.

A useful approximation relating the production rate of ionizing photons to the free–free spectral luminosity L_{ν} at the high frequencies where $\tau \ll 1$ of an HII region in ionization equilibrium is

$$\left(\frac{Q_{\mathrm{H}}}{\mathrm{s}^{-1}} \right) \approx 6.3 \times 10^{52} \left(\frac{T}{10^4 \ \mathrm{K}} \right)^{-0.45} \left(\frac{\nu}{\mathrm{GHz}} \right)^{0.1} \left(\frac{L_{\nu}}{10^{20} \ \mathrm{W \ Hz}^{-1}} \right) . \tag{124}$$

Lecture 16:

5.1 Magnetobremsstrahlung

Gyro radiation $(v \ll c)$
Cyclotron radiation (kinetic energy $\sim$ rest mass $m_e c^2$
Synchrotron radiation (kinetic energy $\gg$ rest mass)

The magnetic force $\vec{F}$ on a particle

$$\vec{F} = \frac{q(\vec{v} \times \vec{B})}{c} \tag{125}$$

is perpendicular to the particle velocity $\vec{v}$ so $\vec{F} \cdot \vec{v} = 0$, $mv^2/2$ is constant, $v_\parallel$ is constant, and $|v_\perp|$ is constant. In a uniform magnetic field, a charged particle moves along a magnetic field line on a helical path with constant linear and angular speeds. In the inertial frame moving with velocity $v_\parallel$, the particle orbits in a circle of radius r perpendicular to the magnetic field with the angular velocity ω needed to balance the centripetal and magnetic forces:

$$m|\dot{v}| = m\omega^2 r = \frac{q}{c}|\vec{v} \times \vec{B}| = \frac{q}{c}\omega r B \ , \tag{126}$$

where the orbital frequency is $\omega = qB/(mc)$. The angular gyro frequency ω_G is *defined* by

$$\omega_G \equiv \frac{qB}{mc} \ . \tag{127}$$

This *definition* holds for *any* particle speed, so the gyro frequency equals the actual orbital frequency if and only if $v \ll c$. The electron gyro frequency $\nu_G = \omega_G/(2\pi)$ is only

$$\left(\frac{\nu_G}{\text{MHz}}\right) = 2.8\left(\frac{B}{\text{gauss}}\right) \ . \tag{128}$$

5.2 Synchrotron power radiated by a single electron
Larmor's equation converted from the electron frame (primed) to the observer's frame:

$$P = P' = \frac{2(e')^2(a'_\perp)^2}{3c^3} = \frac{2e^2(a'_\perp)^2}{3c^3} = \frac{2e^2 a_\perp^2 \gamma^4}{3c^3} = P\frac{2e^2}{3c^3}\gamma^2\frac{e^2 B^2}{m_e^2 c^2}v^2\sin^2\alpha \ , \tag{129}$$

where the constant angle α between the electron velocity $\vec{v}$ and the magnetic field $\vec{B}$ is called the pitch angle. In terms of the Thomson cross section of an electron:

$$\sigma_T \equiv \frac{8\pi}{3}\left(\frac{e^2}{m_e c^2}\right)^2 \approx 6.65 \times 10^{-25} \text{ cm}^2 \tag{130}$$

and the magnetic energy density $U_B = B^2/(8\pi)$, $\quad P = 2\sigma_T \beta^2 \gamma^2 c\, U_B \sin^2\alpha$.
For an isotropic pitch-angle distribution, $\langle \sin^2\alpha \rangle = 2/3$ and the average power is

$$\langle P \rangle = \frac{4}{3}\sigma_T \beta^2 \gamma^2 c U_B \ . \tag{131}$$

5.3 Synchrotron spectrum radiated by a single electron
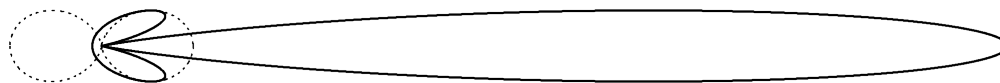
Fig. 13.— Relativistic aberration transforms the dipole power pattern of Larmor radiation in the electron rest frame (dotted curve) into a narrow searchlight beam in the observer's frame. The solid curve is the transformed pattern for $\gamma = 5$. The observed angle between the nulls of the forward beam falls to $\Delta\theta = 2\arcsin(1/\gamma) \approx 2/\gamma$ in the limit $\gamma \gg 1$.
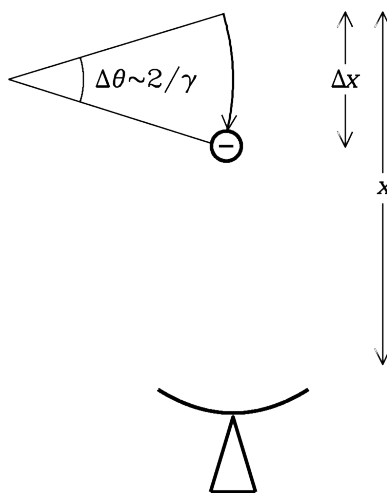
Fig. 14.— The beamed radiation from an ultrarelativistic electron is visible only while the electron's velocity points within $\pm 1/\gamma$ of the line of sight ($\Delta\theta \approx 2/\gamma$). During that time Δt the electron moves $\Delta x = v\Delta t$ toward the observer, almost keeping up with the radiation that moves $c\Delta t$. This shortens the observed pulse duration by a factor $(1 - v/c)$.
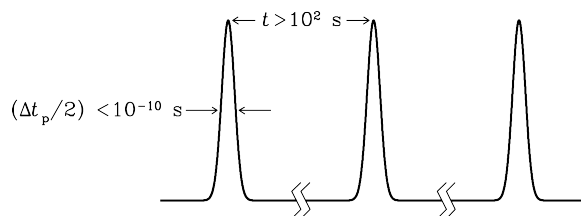
Fig. 15.— Synchrotron radiation is a very spiky series of widely spaced narrow pulses of width $\Delta t_{\rm p} \approx (\gamma^2 \omega_{\rm G} \sin\alpha)^{-1}$. The numerical values on this plot of power versus time correspond to an electron with $\gamma \sim 10^4$ in a magnetic field $B \sim 10\,\mu{\rm G}$.

Most of the synchrotron power appears near the critical frequency

$$\nu_{\rm c} = \frac{3}{2}\gamma^2 \nu_{\rm G}\sin\alpha \ . \tag{132}$$

Lecture 17:

5.3.2 Synchrotron Spectra of Optically Thin Sources

For a source whose relativistic electrons have a power-law energy distribution

$$n(E)dE \propto E^{-\delta}dE \ , \tag{133}$$

each electron emits power

$$P = -\frac{dE}{dt} = \frac{4}{3}\sigma_{\mathrm{T}}\beta^2\gamma^2 cU_B \tag{134}$$

near the frequency

$$\nu \approx \gamma^2 \nu_{\mathrm{G}} \ , \tag{135}$$

and the emission coefficient is

$$j_\nu d\nu = -\frac{dE}{dt}n(E)dE \propto B^{(\delta+1)/2}\nu^{(1-\delta)/2} \ . \tag{136}$$

Thus the [negative] spectral index is $\alpha = -d\ln S/d\ln\nu = (\delta-1)/2$.

5.3.3 Synchrotron Self-Absorption

The effective temperature of an ultrarelativistic electron emitting at frequency ν is

$$T_{\mathrm{e}} \approx \left(\frac{2\pi m_{\mathrm{e}}c\nu}{eB}\right)^{1/2}\frac{m_{\mathrm{e}}c^2}{3k} \approx (1.18 \times 10^6 \ \mathrm{K})\left(\frac{\nu}{\mathrm{Hz}}\right)^{1/2}\left(\frac{B}{\mathrm{gauss}}\right)^{-1/2} \ . \tag{137}$$

At low frequencies, the brightness temperature approaches the effective temperature, the source become optically thick to synchrotron self-absorption. For a uniform cylinder source, $S(\nu) \propto \nu^{5/2}$ and the magnetic field strength can be estimated from the source brightness temperature:

$$\left(\frac{B}{\mathrm{gauss}}\right) \approx 1.4 \times 10^{12}\left(\frac{\nu}{\mathrm{Hz}}\right)\left(\frac{T_{\mathrm{b}}}{\mathrm{K}}\right)^{-2} \ . \tag{138}$$

5.4.1 Minimum Energy and Equipartition

Synchrotron sources contain both relativistic electrons with some energy density U_{e} and a magnetic field with energy density $U_B = B^2/(8\pi)$. For a given synchrotron luminosity L,

$$U_{\mathrm{e}} \propto B^{-3/2} \quad \text{and} \quad U_B \propto B^2 \ . \tag{139}$$

For an ion/electron energy ratio η, the total energy density is

$$U = (1+\eta)U_{\mathrm{e}} + U_B \ . \tag{140}$$

The minimum energy density occurs close to equipartition, when

$$\frac{\text{particle energy density}}{\text{magnetic field energy density}} = \frac{(1+\eta)U_{\mathrm{e}}}{U_B} = \frac{4}{3} \ . \tag{141}$$

The synchrotron lifetime of a source is defined as the ratio of total electron energy E_e to the energy loss rate L from synchrotron radiation: $\tau_s \equiv E_e/L \approx c_{12}B_\perp^{-3/2}$. The factor c_{12} is plotted in *ERA* Figure 5.10.

5.4.2 Eddington Luminosity Limit

At the Eddington luminosity, radiation pressure balances gravity. For ionized hydrogen,

$$\frac{L_E}{4\pi r^2}\frac{\sigma_T}{c} = \frac{GM(m_p + m_e)}{r^2} \approx \frac{GMm_p}{r^2} \ . \tag{142}$$

$$\left(\frac{L_E}{L_\odot}\right) \approx 3.3 \times 10^4 \left(\frac{M}{M_\odot}\right) \ . \tag{143}$$

5.4.3 Application to the Luminous Radio Galaxy Cyg A:
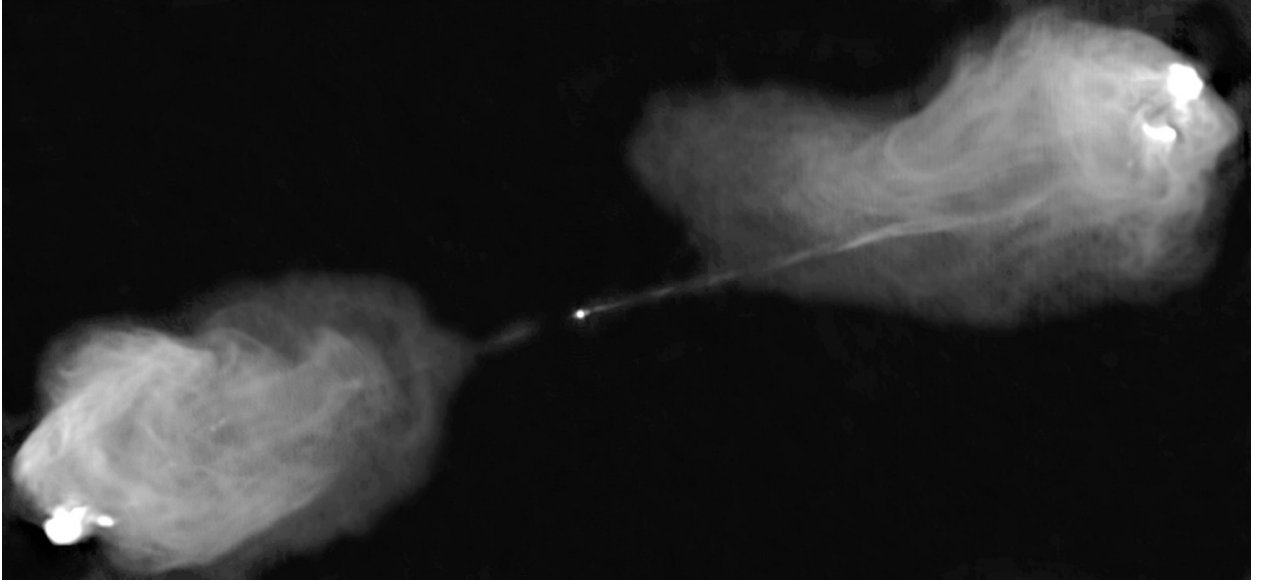
Cyg A is a luminous double radio source with $S_\nu \approx 2000$ Jy$(\nu/\mathrm{GHz})^{-0.8}$ in a peculiar galaxy at distance $d \approx 230$ Mpc. Its radio lobes have radii $R \approx 30$ kpc, and radio luminosity between 10^7 and 10^{11} Hz $L \approx 1.33 \times 10^{45}$ erg s$^{-1} \approx 3.5 \times 10^{11} L_\odot$. The energy source for this radio emission is a compact object at the center of the host galaxy. The Eddington limit (Equation 143) yields a lower limit to its mass $M > 10^7 M_\odot$. The minimum-energy magnetic field strength is $B_{\min} \sim 10^{-4}$ gauss and the corresponding particle energy is $E_{\min} \approx 5 \times 10^{60}$ erg $\sim 3 \times 10^6 M_\odot c^2$, so the compact central source is a supermassive black hole. The synchrotron lifetime is $\tau_s \sim 3 \times 10^6$ yr.

Lecture 18:

5.5 Inverse-Compton Scattering
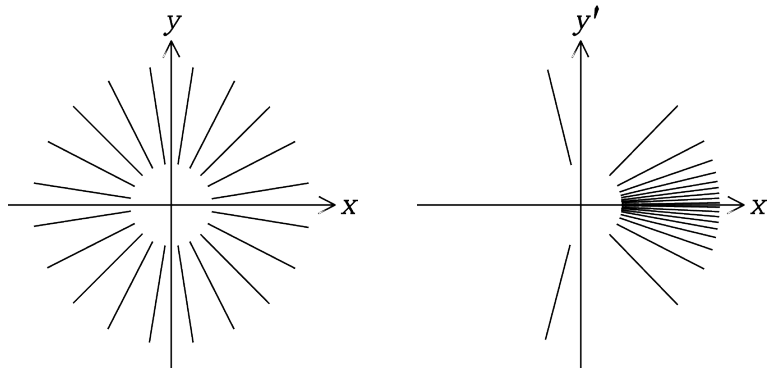
Fig. 16.— For a relativistic electron at rest in the "primed" frame moving with velocity v along the x-axis, the angle of incidence θ' of incoming photons will be much less than the corresponding angle θ in the rest frame of the observer. This figure shows the aberration of an isotropic radiation field (left) seen in a moving frame with $\gamma = (1 - v^2/c^2)^{-1/2} = 5$ (right).

Thomson scattering of this highly anisotropic radiation systematically reduces the electron kinetic energy and converts it into inverse-Compton (IC) radiation by upscattering radio photons to become optical or X-ray photons. Runaway inverse-Compton "cooling" of the relativistic electrons also limits the maximum rest-frame brightness temperature of an incoherent synchrotron source to $T_{\rm b} \approx 10^{12}$ K.

5.5 IC Power from a Single Electron

An electron at rest in an isotropic radiation field of energy density $U_{\rm rad} = |\vec{S}|/c$ will scatter power $P = \sigma_{\rm T} c U_{\rm rad}$, where $\sigma_{\rm T}$ is the Thomson scattering cross section (Equation 130). In the primed frame of an ultrarelativistic electron, $P' = \sigma_{\rm T} c U'_{\rm rad} = P$. In the observer's frame
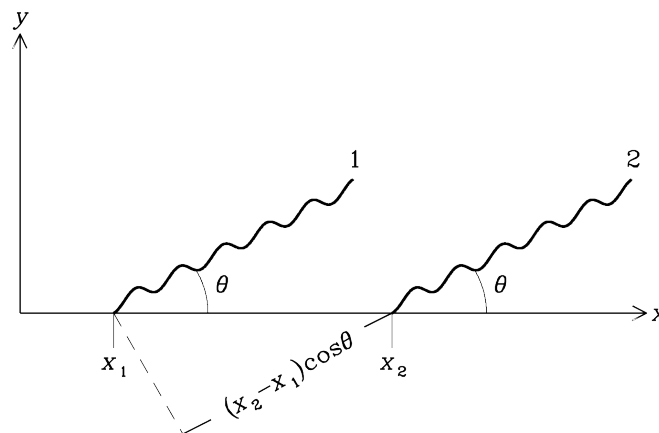
Fig. 17.— Two successive photons striking an electron moving to the right.

shown in Figure 17, the time between the two photon hits is $\Delta t = \Delta t'[\gamma(1 + \beta \cos \theta)]$. Using $\nu = (\Delta t)^{-1}$ yields the relativistic Doppler equation

$$\nu' = \nu[\gamma(1 + \beta \cos \theta)] . \tag{144}$$

In the electron's frame, the frequency ν' and energy $E' = h\nu'$ of each photon are multiplied by $[\gamma(1 + \beta \cos \theta)]$. Moreover, the *rate* at which successive photons arrive is multiplied by the same factor. Thus

$$U'_{\text{rad}} = \frac{U_{\text{rad}}}{4\pi} \int_{\phi=0}^{2\pi} \int_{\theta=0}^{\pi} [\gamma(1 + \beta \cos \theta)]^2 \sin \theta \, d\theta \, d\phi = U_{\text{rad}} \frac{4(\gamma^2 - 1/4)}{3} . \tag{145}$$

The *total* photon power after IC scattering is

$$P_{\text{IC}} = \frac{4}{3} \sigma_{\text{T}} c U_{\text{rad}} \left(\gamma^2 - \frac{1}{4} \right) - \sigma_{\text{T}} c U_{\text{rad}} = \frac{4}{3} \sigma_{\text{T}} c U_{\text{rad}} (\gamma^2 - 1) . \tag{146}$$

Subtracting the *initial* photon power $\sigma_{\text{T}} c U_{\text{rad}}$ gives the *net* IC power

$$P_{\text{IC}} = \frac{4}{3} \sigma_{\text{T}} c \beta^2 \gamma^2 U_{\text{rad}} . \tag{147}$$

The ratio of IC to synchrotron power is simply

$$\frac{P_{\text{IC}}}{P_{\text{syn}}} = \frac{U_{\text{rad}}}{U_B} . \tag{148}$$

The IC loss is proportional to the radiation energy density and the synchrotron loss is proportional to the magnetic energy density. Note that synchrotron and inverse-Compton losses have the same electron-energy dependence ($dE/dt \propto \gamma^2$), so their effects on radio spectra are indistinguishable.

IC scattering by an electron with Lorentz factor γ boosts the photon frequency from ν_0 up to

$$\frac{\nu_{\text{max}}}{\nu_0} \approx 4\gamma^2 \qquad \text{and} \qquad \frac{\langle \nu \rangle}{\nu_0} = \frac{4}{3} \gamma^2 . \tag{149}$$

Because the IC spectrum of a single electron is sharply peaked, the IC spectrum of a source with electron-energy distribution $n(E) \propto E^{-\gamma}$ will be a power law with spectral index

$$\alpha = \frac{\delta - 1}{2} , \tag{150}$$

which is the same as that of synchrotron emission.

Synchrotron self-Compton radiation results from inverse-Compton scattering of synchrotron radiation by the same relativistic electrons that produced the synchrotron radiation. Self-Compton scattering adds to U_{rad} and in bright sources can cause significant second-order scattering, a runaway process that strongly cools relativistic electrons in sources significantly brighter than

$$T_{\text{max}} \sim 10^{12} \text{ K} . \tag{151}$$

This limits the rest-frame brightness of incoherent synchrotron radiation.

Lecture 19:

5.6 Extragalactic Radio Sources
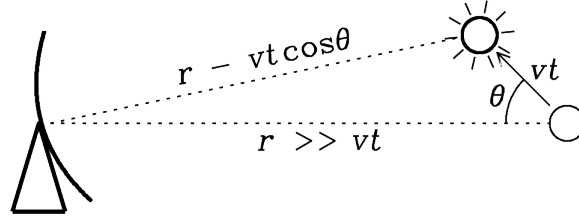
Fig. 18.— A source moving with speed $v < c$ at an angle $\theta < \pi/2$ from the line of sight may appear to be moving faster than c in projection onto the sky because the light travel time is reduced by $vt \cos \theta / c$ during time t.

The *apparent* transverse velocity of the moving component is

$$\beta_\perp(\text{apparent}) = \frac{\beta \sin \theta}{1 - \beta \cos \theta} \ . \tag{152}$$

For any component speed $\beta < 1$, the angle $\theta_{\rm m} = \cos^{-1}(\beta) = \sin^{-1}(1/\gamma)$ yields the maximum *apparent* transverse velocity

$$\max[\beta_\perp(\text{apparent})] = \frac{\beta(1 - \beta^2)^{1/2}}{1 - \beta^2} = \beta\gamma \ , \tag{153}$$

which can be "superluminal": $\beta_\perp(\text{apparent}) > 1$.

The relativistic Doppler formula (*ERA* Equation 144) relates the frequency ν' emitted in the component frame to the observed frequency ν. Defining θ as the angle between the line of sight and the velocity of an *approaching* component,

$$\nu = \frac{\nu'}{\gamma(1 - \beta \cos \theta)} \ . \tag{154}$$

The Doppler factor δ defined by

$$\delta \equiv [\gamma(1 - \beta \cos \theta)]^{-1} = \frac{\nu}{\nu'} \tag{155}$$

can range from $(2\gamma)^{-1}$ to 2γ. At $\theta = \pi/2$ the transverse Doppler shift is $\delta = \nu/\nu' = 1/\gamma$.

The observed flux density S of a relativistically moving component emitting isotropically in its rest frame depends critically on its Doppler factor δ. The exact amount of Doppler boosting caused by relativistic beaming is somewhat model dependent but probably lies in the range

$$\delta^{2+\alpha} < \frac{S}{S_0} < \delta^{3+\alpha} \ , \tag{156}$$

where S_0 would be the flux density if the source were stationary and $\alpha = -d \log S / d \log \nu$ is the (negative) spectral index.

5.6.2 Unified Models: AGN orientation effects—beaming and dust absorption.
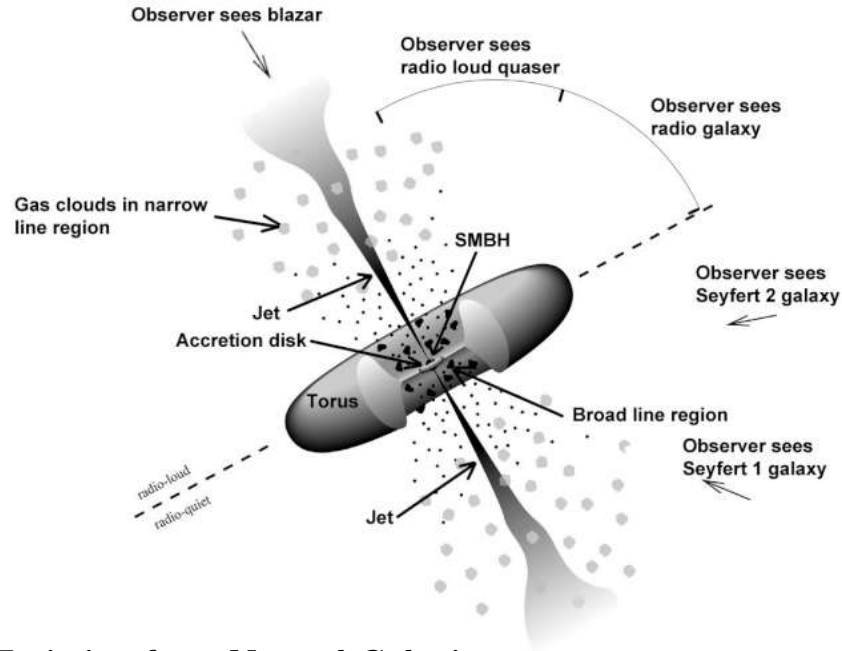
5.6.3 Radio Emission from Normal Galaxies

The radio emission from a "normal" galaxy is powered by (1) free–free emission from HII regions ionized by short-lived $M > 15 M_\odot$ stars and (2) synchrotron radiation from cosmic-ray electrons accelerated in the supernova remnants of short-lived $M > 8 M_\odot$ stars. It is correlated with far-infrared emission and is an extinction-free tracer of recent star formation.

5.6.4 Extragalactic Radio Source Populations and Cosmological Evolution
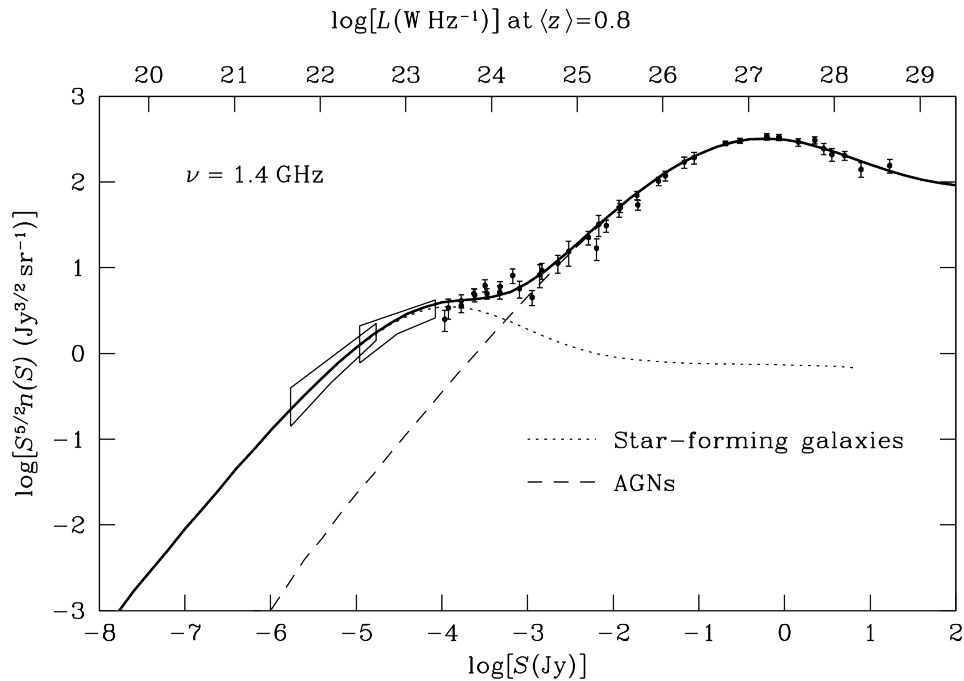
Lecture 20:

6.1 Pulsar Properties

Pulsars are magnetized neutron stars that appear to emit periodic short pulses of radio radiation with periods between 1.4 ms and 23.5 s. The name pulsar blends "pulse" and "star," but pulsars are not pulsating stars. Like lighthouses, they continuously emit rotating beams of radiation and appear to flash each time the beam sweeps across the observer's line of sight. They were discovered serendipitously by Cambridge University graduate student Jocelyn Bell, who noticed that "scruffy" pulses in her chart-recorder data repeated every sidereal day, so they were not likely terrestrial interference.

Neutron stars are physics laboratories sampling extreme conditions—deep gravitational potentials $GM/(rc^2) \sim 1$, densities $\rho \sim 10^{14}$ g cm^{-3} exceeding those in atomic nuclei, and magnetic field strengths as high as $B \sim 10^{14}$ or even 10^{15} gauss—not found on Earth.

Pulse periods P can be timed with fractional errors as small as 10^{-16}. Accurate pulsar timing permits exquisitely sensitive measurements of quantities such as the power of gravitational radiation emitted by a pulsar in a binary system, neutron-star masses, general relativistic effects in strong gravitational fields, orbital perturbations from binary companions as light as planets, accurate pulsar positions and proper motions, and potentially the distortions of interstellar space produced by long-wavelength gravitational radiation from the mergers of supermassive black holes throughout the universe.

A nearly spherical star with mass M, radius R, and angular velocity $\Omega = 2\pi/P$ must have equatorial centrifugal acceleration less than gravitational acceleration

$$\Omega^2 R < \frac{GM}{R^2} \qquad \text{so} \qquad P^2 > \left(\frac{4\pi R^3}{3}\right)\frac{3\pi}{GM} = \frac{3\pi}{G\rho} \quad \text{and} \quad R < \left(\frac{GMP^2}{4\pi^2}\right)^{1/3}. \qquad (157)$$

The "canonical" or typical neutron star parameters are mass $\approx$ Chandrasekhar mass $M \approx 1.4 M_\odot$, radius $R \approx 10$ km, and moment of inertia $I = 2MR^2/5 \approx 10^{45}$ g cm^2.

Flux conservation during the core collapse of a massive star yields enormous pulsar magnetic fields $B \sim 10^{12}$ G. If the magnetic dipole axis is mis-aligned by angle α from the spin axis of a neutron star, the magnetic-field equivalent of Larmor's equation is

$$P_{\text{rad}} = \frac{2}{3}\frac{(\ddot{m}_\perp)^2}{c^3}, \qquad (158)$$

where $m_\perp = m\sin\alpha$ is the perpendicular component of the magnetic dipole moment, which is $m = BR^3$ for a uniformly magnetized sphere. If the neutron star rotates with angular velocity $\Omega = 2\pi/P$, then

$$P_{\text{rad}} = \frac{2}{3}\frac{m_\perp^2 \Omega^4}{c^3} = \frac{2}{3c^3}(BR^3\sin\alpha)^2\left(\frac{2\pi}{P}\right)^4, \qquad (159)$$

where P is the pulsar period. This magnetic dipole radiation will appear at the *very* low radio frequency $\nu = P^{-1} < 1$ kHz, so low that it cannot propagate through the surrounding ionized nebula or ISM. Magnetic dipole radiation extracts rotational kinetic energy from the neutron star and causes the pulsar period to increase with time. The absorbed radiation deposits energy in the surrounding nebula, the Crab Nebula being a prime example.

The rotational kinetic energy of a neutron star is

$$E = \frac{I\Omega^2}{2} = \frac{2\pi^2 I}{P^2} \tag{160}$$

and the spin-down luminosity is

$$-\dot{E} \equiv -\frac{dE_{\rm rot}}{dt} = -\frac{d}{dt}\left(\frac{1}{2}I\Omega^2\right) = -I\Omega\dot{\Omega} = \frac{4\pi^2 I\dot{P}}{P^3} \ . \tag{161}$$

The Crab pulsar has $P = 0.033$ s and $\dot{P} = 10^{-12.4}$. If $I = 10^{45}$ g cm^2, its spin-down luminosity is $-\dot{E} \approx 4 \times 10^{38}$ erg s$^{-1} \approx 10^5 L_\odot$!

If $P_{\rm rad} = -\dot{E}$, the minimum magnetic field strength at the neutron star surface is

$$B > \left(\frac{3c^3 I}{8\pi^2 R^6}\right)^{1/2} (P\dot{P})^{1/2} \ . \tag{162}$$

For a canonical pulsar

$$\left(\frac{B}{\rm gauss}\right) > 3.2 \times 10^{19} \left(\frac{P\dot{P}}{\rm s}\right)^{1/2} \ . \tag{163}$$

If the spin-down luminosity equals the magnetic dipole radiation luminosity and $(B\sin\alpha)$ doesn't vary, a pulsar's age τ can be estimated from $P\dot{P}$ on the further assumption that the pulsar's initial period $P_0 \ll P$ today. Solving *ERA* Equation 6.23 for $P\dot{P}$ shows that

$$P\dot{P} = \frac{8\pi^2 R^6 (B\sin\alpha)^2}{3c^3 I} \tag{164}$$

doesn't vary. In the limit $P_0^2 \ll P^2$, the characteristic age of a pulsar *defined* by

$$\tau \equiv \frac{P}{2\dot{P}} \tag{165}$$

should be close to the actual age of the pulsar. In the case of the Crab pulsar of 1054 AD, $\tau \approx 1300$ yr is close to the known age.

If $P_{\rm rad} = -\dot{E}$ then Equations 159 and 161 together imply $\dot{\Omega} \propto \Omega^3$. The braking index n defined by $\dot{\Omega} \propto \Omega^n$ can be measured via

$$n = 2 - \frac{P\ddot{P}}{\dot{P}^2} \ . \tag{166}$$

Braking indices in the range $1.4 \leq n < 3$ have been observed.

The P$\dot{P}$ diagram (*ERA* Figure 6.3) follows the lives of pulsars, their characteristic ages, and their minimum magnetic field strengths.

Lecture 21:

6.2 Pulsars and the Interstellar Medium

The electrons in the ISM make up a cold plasma whose refractive index is

$$\mu = \left[1 - \left(\frac{\nu_{\mathrm{p}}}{\nu}\right)^2\right]^{1/2} , \tag{167}$$

where ν is the frequency of the radio waves, ν_{p} is the plasma frequency

$$\nu_{\mathrm{p}} = \left(\frac{e^2 n_{\mathrm{e}}}{\pi m_{\mathrm{e}}}\right)^{1/2} \approx 8.97 \text{ kHz} \left(\frac{n_{\mathrm{e}}}{\mathrm{cm}^{-3}}\right)^{1/2} \tag{168}$$

and n_{e} is the electron number density. For a typical ISM value $n_{\mathrm{e}} \sim 0.03 \text{ cm}^{-3}$, $\nu_{\mathrm{p}} \sim 1.5 \text{ kHz}$. The pulse group velocity is $\nu_{\mathrm{g}} = \mu c$, so the dispersion delay is

$$\left(\frac{t}{\sec}\right) \approx 4.149 \times 10^3 \left(\frac{\mathrm{DM}}{\mathrm{pc} \ \mathrm{cm}^{-3}}\right) \left(\frac{\nu}{\mathrm{MHz}}\right)^{-2} , \tag{169}$$

where

$$\mathrm{DM} \equiv \int_0^d n_{\mathrm{e}} \, dl \tag{170}$$

in units of pc cm^{-3} is called the dispersion measure. Crude distances to pulsars can be estimated from their DMs by using $n_{\mathrm{e}} \sim 0.03 \text{ cm}^{-3}$. Inhomogeneities in the ISM cause intensity fluctuations or scintillations of pulsar signals, and ray scattering causes pulse broadening $\propto \nu^{-4}$.

Uncorrected differential delays across the observing band cause dispersive smearing of pulses.

6.3 Pulsar Timing

Pulsar timing is the regular monitoring of the rotation period of the neutron star by precisely tracking the pulse arrival times to *unambiguously account for every rotation of the pulsar over long periods (years to decades) of time.*

The instantaneous pulse frequency is $f = 1/P$, and the instantaneous pulse phase ϕ is defined by $d\phi/dt = f$. Pulse phase is usually measured in *turns* of 2π radians, so $0 < \phi < 1$. For timing, the average pulse profile is correlated with a template or model profile so that its phase offset can be determined. When multiplied by the instantaneous pulse period, that phase yields a time offset that can be added to a high-precision reference point on the profile (for example, the left edge of the profile based on the recorded time of the first sample of the observation) to create the time of arrival (TOA). In the nearly inertial frame of the Solar System barycenter (center of mass), the rotation period of a pulsar is nearly constant, so $\phi(t)$ can be approximated by the Taylor expansion

$$\phi(t) = \phi_0 + f(t - t_0) + \frac{1}{2}\dot{f}(t - t_0)^2 + \cdots , \tag{171}$$

where ϕ_0 and t_0 are arbitrary reference phases and times for each pulsar. The critical constraint for pulsar timing is that *the observed rotational phase difference between each of the TOAs must contain an integer number of rotations.* Many corrections have to be applied to the observed TOAs before $\phi(t)$ can be expressed as a Taylor series (Equation 171); e.g.,

$$t = t_\mathrm{t} - t_0 + \Delta_\mathrm{clock} - \Delta_\mathrm{DM} + \Delta_\mathrm{R\odot} + \Delta_\mathrm{E\odot} + \Delta_\mathrm{S\odot} + \Delta_\mathrm{R} + \Delta_\mathrm{E} + \Delta_\mathrm{S} \;, \qquad (172)$$

where Δ_clock is the observatory clock correction, $\Delta_\mathrm{R\odot} \approx 500\cos\beta$ s is the Roemer light travel delay across the Earth's orbit for a pulsar at ecliptic latitude β, etc. Pulsar position errors $\Delta\lambda$ in ecliptic longitude and $\Delta\beta$ in ecliptic latitude can be measured with sub-arcsec accuracy via pulsar timing. Roemer delays across the orbits of binary pulsars yield accurate measures of the pulsar orbital parameters including small post-Keplerian relativistic effects. Timing measurements of orbital decay in the Hulse-Taylor binary pulsar B1913+16 showed that its orbit is decaying as predicted by general relativity for the emission of gravitational radiation. The double-pulsar binary J0737$-$3039 contains two pulsar clocks whose timing has demonstrated the accuracy of general relativity and determined the masses of both pulsars. Pulsar timing arrays (PTAs) are likely to detect the low-frequency (nHz) gravitational-wave background from merging supermassive black-hole binaries in the near future.

Lecture 22:

7.1 Spectral Lines

Spectral lines are narrow ($\Delta\nu \ll \nu$) emission or absorption features in the spectra of gaseous and ionized sources: recombination lines of ionized hydrogen and heavier atoms, rotational lines of polar molecules such as CO, and the $\lambda = 21$ cm hyperfine line of interstellar HI.

Spectral-line emission and absorption are intrinsically quantum phenomena. Particles of momentum p have De Broglie wavelengths $\lambda = h/p$, where Planck's constant $h \approx 6.63 \times 10^{-27}$ erg s has dimensions of action (m l² t), the same as energy×time or angular momentum. Stimulated emission is important at radio frequencies $h\nu \ll kT$.

7.2.1 Recombination Line Frequencies
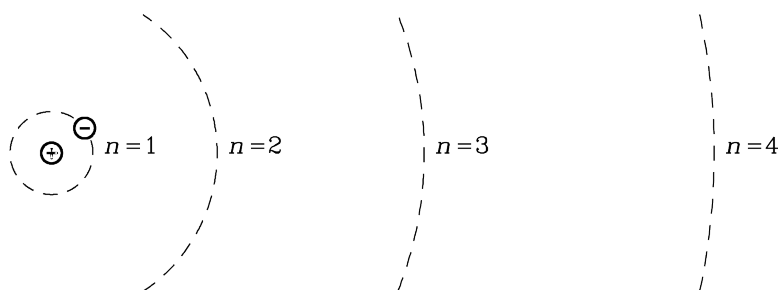
In the Bohr model of the hydrogen atom, the circular electron orbits have circumferences $n\lambda$ corresponding to standing waves. The Bohr radius a_n of the nth permitted orbit obeys

$$2\pi a_n = n\lambda = n\frac{h}{p} = \frac{nh}{m_e v} \ , \tag{173}$$

where n is called the principal quantum number. The Coulomb and centrifugal forces must balance: $e^2/a_n^2 = m_e v^2/a_n$. Then, in terms of the reduced Planck's constant $\hbar \equiv h/(2\pi)$,

$$a_n = \frac{n^2 \hbar^2}{m_e e^2} = \frac{[6.63/(2\pi) \times 10^{-27} \text{ erg s}]^2}{9.11 \times 10^{-28} \text{ g} \cdot (4.8 \times 10^{-10} \text{ statcoul})^2} n^2 \approx 0.53 \times 10^{-8} \text{ cm} \cdot n^2 \ . \tag{174}$$

The electron in a Bohr atom can fall from the level $(n + \Delta n)$ to n, where Δn and n are any natural numbers (1, 2, 3, ...), by emitting a photon whose energy $\Delta E = h\nu$ equals the energy difference between the initial and final levels.

$$E_n = T + V = -T = V/2 = -\frac{e^2}{2a_n} = -e^2 \left(\frac{m_e e^2}{2n^2 \hbar^2}\right) = -\left(\frac{m_e e^4}{2\hbar^2}\right)\frac{1}{n^2} \tag{175}$$

so

$$\nu = \left(\frac{2\pi^2 m_e e^4}{h^3 c}\right) c \left[\frac{1}{n^2} - \frac{1}{(n+\Delta n)^2}\right] . \tag{176}$$

The factor in large parentheses is the Rydberg constant $R_\infty = 1.09737312\ldots \times 10^5$ cm^{-1} and $R_\infty c = 3.28984\ldots \times 10^{15}$ Hz is the Rydberg frequency. For a finite nuclear mass $M \gg m_e$,

$$\nu = R_M c \left[\frac{1}{n^2} - \frac{1}{(n+\Delta n)^2}\right] , \qquad \text{where} \qquad R_M \equiv R_\infty \left(1 + \frac{m_e}{M}\right)^{-1} . \tag{177}$$

7.2.2 Recombination Line Strengths

The spontaneous emission rate is the average rate at which an isolated atom emits photons. Radio photons are emitted by atoms with $n \gg 1$, so we can invoke the correspondence principle, Bohr's hypothesis that systems with large quantum numbers behave almost classically, and use the classical Larmor's formula to calculate the time-averaged radiated power $\langle P \rangle$ for an electric dipole with dipole moment ea_n:

$$\langle P \rangle = \frac{2e^2}{3c^3}(\omega^2 a_n)^2 \langle \cos^2(\omega t) \rangle = \frac{2e^2}{3c^3}(2\pi\nu)^4 \frac{a_n^2}{2} \ . \tag{178}$$

The photon emission rate (s^{-1}) equals the average power emitted by one atom divided by the energy of each photon. The spontaneous emission rate for transitions from level n to level $(n-1)$ is denoted by $A_{n,n-1}$:

$$A_{n,n-1} = \frac{\langle P \rangle}{h\nu} \ , \quad \text{where} \quad \nu \approx \frac{2R_\infty c \Delta n}{n^3} \tag{179}$$

in the limit $\Delta n \ll n$. In that limit, $A_{n+1,n} \approx A_{n,n-1}$ also. After some algebra,

$$A_{n+1,n} \approx \frac{\langle P \rangle}{h\nu} \approx \left(\frac{64\pi^6 m_e e^{10}}{3c^3 h^6} \right) \frac{1}{n^5} \approx 5.3 \times 10^9 \left(\frac{1}{n^5} \right) \ \mathrm{s}^{-1} \ . \tag{180}$$

For example, the 5.0089 GHz H109α transition rate is $A_{110,109} \approx 0.3 \ \mathrm{s}^{-1}$. The corresponding natural line width $\Delta\nu \sim A_{n+1,n}/\pi \sim 0.1$ Hz is much less than the collisional broadening and very much less than the line width caused by Doppler shifts reflecting radial velocities v_r. If $v_r \ll c$, then $\nu \approx \nu_0(1 - v_r/c)$.
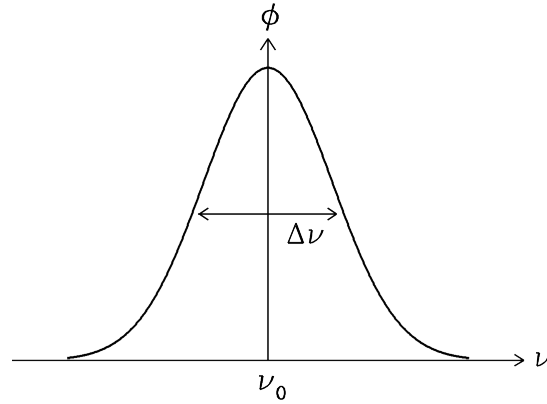
Thermal gas in LTE has a Maxwellian velocity distribution given by *ERA* Equation B.49, so its normalized line profile $\phi(\nu)$ is the Gaussian

$$\phi(\nu) = \frac{c}{\nu_0}\left(\frac{M}{2\pi kT} \right)^{1/2} \exp\left[-\frac{Mc^2}{2kT}\frac{(\nu - \nu_0)^2}{\nu_0^2} \right] \tag{181}$$

characterized by its half-power width $\Delta\nu$ and peak height $\phi(\nu_0)$:

$$\Delta\nu = \left[\frac{8\ln(2)\,k}{c^2} \right]^{1/2} \left(\frac{T}{M} \right)^{1/2} \nu_0 \quad \text{and} \quad \phi(\nu_0) = \left(\frac{\ln 2}{\pi} \right)^{1/2} \frac{2}{\Delta\nu} \ . \tag{182}$$

Lecture 23:

7.3.1 Einstein Coefficients
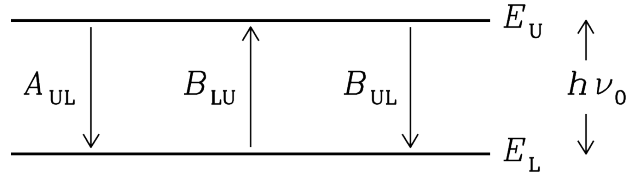
The three Einstein coefficients for a two-level system are:

(1) A_{UL} is the spontaneous emission rate (s^{-1}) per atom or molecule.

(2) B_{LU}, multiplied by the line-profile weighted mean radiation energy density

$$\bar{u} \equiv \int_0^\infty u_\nu(\nu)\,\phi(\nu)\,d\nu \;, \tag{183}$$

is the absorption rate (s^{-1}) per atom or molecule in the lower energy state.

(3) B_{UL} multiplied by $\bar{u}$ is the stimulated emission (or negative absorption) rate (s^{-1}) per atom or molecule in the upper energy state. Stimulated emission is the emission of a second photon with the same energy and direction as the incident photon.

Thermodynamic equilibrium (TE) is a stationary state, so in a system with atomic or molecular density n_{U} in the upper energy state and n_{L} in the lower energy state, the rate of photon creation must equal the rate of photon destruction:

$$n_{\mathrm{U}}(A_{\mathrm{UL}} + B_{\mathrm{UL}}\bar{u}) = n_{\mathrm{L}}B_{\mathrm{LU}}\bar{u} \;. \tag{184}$$

In TE, the Boltzmann equation relates n_{U} and n_{L}:

$$\frac{n_{\mathrm{U}}}{n_{\mathrm{L}}} = \frac{g_{\mathrm{U}}}{g_{\mathrm{L}}}\,\exp\left[-\frac{(E_{\mathrm{U}} - E_{\mathrm{L}})}{kT}\right] = \frac{g_{\mathrm{U}}}{g_{\mathrm{L}}}\,\exp\left(-\frac{h\nu_0}{kT}\right) \;, \tag{185}$$

where g_{U} and g_{L} are the statistical weights equal to the number of distinct states having those energies. In TE, $\bar{u} = (4\pi/c)B_\nu(\nu_0)$ and

$$\bar{u} = \frac{A_{\mathrm{UL}}}{(n_{\mathrm{L}}/n_{\mathrm{U}})B_{\mathrm{LU}} - B_{\mathrm{UL}}} = A_{\mathrm{UL}}\left[\frac{g_{\mathrm{L}}}{g_{\mathrm{U}}}\exp\left(\frac{h\nu_0}{kT}\right)B_{\mathrm{LU}} - B_{\mathrm{UL}}\right]^{-1} \approx \frac{4\pi}{c}\frac{2h\nu_0^3}{c^2}\left[\exp\left(\frac{h\nu_0}{kT}\right) - 1\right]^{-1}. \tag{186}$$

The equation

$$\frac{A_{\mathrm{UL}}}{B_{\mathrm{UL}}}\left[\frac{g_{\mathrm{L}}}{g_{\mathrm{U}}}\frac{B_{\mathrm{LU}}}{B_{\mathrm{UL}}}\exp\left(\frac{h\nu_0}{kT}\right) - 1\right]^{-1} = \frac{8\pi h\nu_0^3}{c^3}\left[\exp\left(\frac{h\nu_0}{kT}\right) - 1\right]^{-1} \tag{187}$$

is unusual because it is true for *all* T. Consequently, the temperature-independent parts (outside the brackets) must be equal *and* the temperature-dependent parts (inside the brackets) must be equal, yielding the two equations of detailed balance

$$\frac{g_{\mathrm{L}}}{g_{\mathrm{U}}}\frac{B_{\mathrm{LU}}}{B_{\mathrm{UL}}} = 1 \quad \text{and} \quad \frac{A_{\mathrm{UL}}}{B_{\mathrm{UL}}} = \frac{8\pi h\nu_0^3}{c^3} \tag{188}$$

that determine both B_{UL} and B_{LU} in terms of A_{UL} for *any* system, even if not in TE or LTE.

7.3.2 Line Radiative Transfer and Detailed Balance

$$\frac{dI_\nu}{ds} = -\kappa I_\nu + j_\nu = -\left(\frac{h\nu_0}{c}\right)n_{\mathrm{L}}B_{\mathrm{LU}}\phi(\nu)I_\nu + \left(\frac{h\nu_0}{c}\right)n_{\mathrm{U}}B_{\mathrm{UL}}\phi(\nu)I_\nu + \left(\frac{h\nu_0}{4\pi}\right)n_{\mathrm{U}}A_{\mathrm{UL}}\phi(\nu) \quad (189)$$

$$= -\left(\frac{h\nu_0}{c}\right)(n_{\mathrm{L}}B_{\mathrm{LU}} - n_{\mathrm{U}}B_{\mathrm{UL}})\phi(\nu)I_\nu + \left(\frac{h\nu_0}{4\pi}\right)n_{\mathrm{U}}A_{\mathrm{UL}}\phi(\nu) \quad (190)$$

In LTE, the *net* line opacity coefficient can be written in terms of A_{UL} only:

$$\kappa(\nu) = \frac{c^2}{8\pi\nu_0^2}\frac{g_{\mathrm{U}}}{g_{\mathrm{L}}}n_{\mathrm{L}}A_{\mathrm{UL}}\left[1 - \exp\left(-\frac{h\nu_0}{kT}\right)\right]\phi(\nu) \; . \quad (191)$$

The two terms in brackets represent ordinary and negative opacity, respectively. In the Rayleigh-Jeans limit $h\nu \ll kT$, the net opacity $\propto T^{-1}$ and $B_\nu \propto T$, so $\kappa B_\nu \propto T^0$ and the brightness of an optically thin ($\tau \ll 1$) radio emission line is proportional to the column density of emitting gas but can be nearly independent of the gas temperature.

Even if a two-level system is not in LTE, its excitation temperature T_{x} is *defined* by

$$\frac{n_{\mathrm{U}}}{n_{\mathrm{L}}} \equiv \frac{g_{\mathrm{U}}}{g_{\mathrm{L}}}\exp\left(-\frac{h\nu_0}{kT_{\mathrm{x}}}\right) \; . \quad (192)$$

In a two-level system, T_{x} is determined by a balance between radiative and collisional excitations and de-excitations. If collisions cause $n_{\mathrm{L}}C_{\mathrm{LU}}$ excitations per unit volume per unit time from the lower level to the upper level and $n_{\mathrm{U}}C_{\mathrm{UL}}$ de-excitations per unit volume per unit time from the upper level to the lower level, then Equation 184 becomes

$$n_{\mathrm{U}}(A_{\mathrm{UL}} + B_{\mathrm{UL}}\bar{u} + C_{\mathrm{UL}}) = n_{\mathrm{L}}(B_{\mathrm{LU}}\bar{u} + C_{\mathrm{LU}}) \; . \quad (193)$$

If the spontaneous emission rate is much larger than the collision rate, $T_{\mathrm{x}} \to T_{\mathrm{b}}$; if the collision rate is much higher than the spontaneous emission rate, $T_{\mathrm{x}} \to T_{\mathrm{k}}$. For any A_{UL} and C_{UL}, T_{x} lies between T_{k} and T_{b}.

7.5 Masers

If the upper energy level is *overpopulated* ($n_{\mathrm{U}}/n_{\mathrm{L}} > g_{\mathrm{U}}/g_{\mathrm{L}}$), then $T_{\mathrm{x}} < 0$ and the net line opacity coefficient (Equation 191) is negative. This implies brightness gain instead of loss; the intensity of a background source at frequency ν_0 will be amplified.

Maser emission quickly depopulates the upper energy level, so masers have to be "pumped" to emit continuously. Typically one or more higher energy levels absorb radiation from a pump source (e.g., infrared continuum from a star or an AGN), and radiative decays preferentially repopulate the upper energy level. This radiative pumping process produces no more than one maser photon per pump photon, so the pump energy required is proportional to the frequency $\nu = E/h$ of the pump photon. If the maser photon emission rate is limited by the pump luminosity, the maser is described as being saturated; if the pump power is more than adequate, the maser is unsaturated. Collisions can also pump masers.

Lecture 24:

7.6. Recombination Line Sources in LTE

The net line opacity coefficient for the $n \to n+1$ hydrogen recombination line in LTE is obtained by combining Equation 191 for the net line absorption coefficient with the Saha equation

$$n_n = n^2 \left(\frac{h^2}{2\pi m_e k T_e} \right)^{3/2} n_p n_e \exp\left(\frac{\chi_n}{kT_e} \right) , \tag{194}$$

where $\chi_n < 0$ is the ionization potential of the nth energy level. For large n, $|\chi_n| \ll kT_e$ and the exponential factor $\exp[\chi_n/(kT_e)] \approx 1$ can be ignored. At the line center frequency ν_0 it is

$$\kappa(\nu_0) \approx \left(\frac{n_e^2}{T_e^{5/2} \Delta\nu} \right) \left(\frac{4\pi e^6 h}{3 m_e^{3/2} k^{5/2} c} \right) \left(\frac{\ln 2}{2} \right)^{1/2} \tag{195}$$

for any level $n \gg 1$.

The optical depth $\tau_L = \int \kappa \, ds$ at the line center frequency ν_0 can be expressed in terms of the emission measure EM defined by Equation 121. In astronomically convenient units,

$$\tau_L \approx 1.92 \times 10^3 \left(\frac{T_e}{K} \right)^{-5/2} \left(\frac{EM}{pc\,cm^{-6}} \right) \left(\frac{\Delta\nu}{kHz} \right)^{-1} . \tag{196}$$

Because $\tau_L \ll 1$ in all known HII regions, the brightness temperature contributed by a recombination *emission* line at its center frequency ν_0 is

$$T_L \approx T_e \tau_L \approx 1.92 \times 10^3 \left(\frac{T_e}{K} \right)^{-3/2} \left(\frac{EM}{pc\,cm^{-6}} \right) \left(\frac{\Delta\nu}{kHz} \right)^{-1} . \tag{197}$$

At frequencies high enough that the free–free continuum is also optically thin, the peak line-to-continuum ratio (which occurs at frequency ν_0) in LTE is

$$\frac{T_L}{T_C} \approx 7.0 \times 10^3 \left(\frac{\Delta v}{km\,s^{-1}} \right)^{-1} \left(\frac{\nu}{GHz} \right)^{1.1} \left(\frac{T_e}{K} \right)^{-1.15} \left[1 + \frac{N(He^+)}{N(H^+)} \right]^{-1} , \tag{198}$$

where Δv is the line FWHM expressed as a velocity and the typical He^+/H^+ ion ratio is $N(He^+)/N(H^+) \approx 0.08$. The term in square brackets is necessary because He^+ contributes to the free–free continuum emission but not to the hydrogen recombination line.

The line-to-continuum ratio yields an estimate of the electron temperature T_e that is independent of the emission measure so long as the frequency is high enough that the continuum optical depth is small:

$$\left(\frac{T_e}{K} \right) \approx \left[7.0 \times 10^3 \left(\frac{\nu}{GHz} \right)^{1.1} 1.08^{-1} \left(\frac{\Delta v}{km\,s^{-1}} \right)^{-1} \left(\frac{T_C}{T_L} \right) \right]^{0.87} . \tag{199}$$

7.7.1 Molecular Line Frequencies
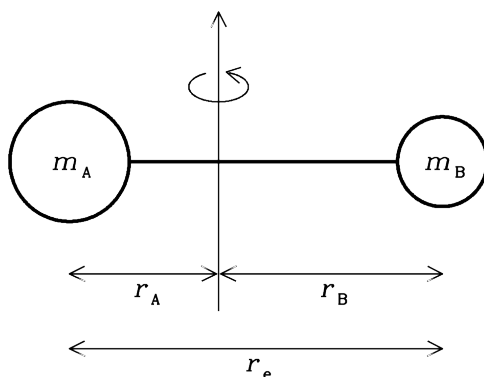
The permitted rotation rates of diatomic molecules are determined by the quantization of angular momentum $L = n\hbar$, $n = 1, 2, 3, \ldots$

In the inertial center-of-mass frame, $L = I\omega$, where I is the moment of inertia and ω is the angular velocity of rotation. Nearly all of the mass is in the two compact (much smaller than r_e) nuclei, so $I = (m_A r_A^2 + m_B r_B^2)$, $L = (m_A r_A^2 + m_B r_B^2)\omega$, and

$$L = \left(\frac{m_A m_B}{m_A + m_B}\right) r_e^2 \omega = m r_e^2 \omega \;, \tag{200}$$

where

$$m \equiv \left(\frac{m_A m_B}{m_A + m_B}\right) \tag{201}$$

is the reduced mass of the molecule. The rotational kinetic energy is $E_{\rm rot} = I\omega^2/2$. The quantization of angular momentum to integer multiples of $\hbar$ implies that rotational energy is also quantized. The corresponding energy eigenvalues of the Schrödinger equation are

$$E_{\rm rot} = \left(\frac{\hbar^2}{2I}\right) J(J+1) \;, \qquad J = 0, 1, 2, \ldots \tag{202}$$

The changes in rotational energy are restricted by the quantum-mechanical selection rule $\Delta J = \pm 1$. Going from J to $J - 1$ releases energy

$$\Delta E_{\rm rot} = [J(J+1) - (J-1)J]\frac{\hbar^2}{2I} = \frac{\hbar^2 J}{I} \;. \tag{203}$$

The frequency of the photon emitted during this rotational transition is

$$\nu = \frac{\Delta E_{\rm rot}}{h} = \frac{\hbar J}{2\pi I} = \frac{hJ}{4\pi^2 m r_e^2}, \qquad J = 1, 2, \ldots \tag{204}$$

Thus a plot of the radio spectrum of a particular molecular species in an interstellar cloud will look like a ladder whose steps are all harmonics of the fundamental frequency that is determined solely by the moment of inertia $I = m r_e^2$ of that species. Nonlinear molecules such as the symmetric-top ammonia (NH_3) with two distinct rotational axes have more complex spectra consisting of many parallel ladders.

Lecture 25:

7.7.2 Molecular Excitation

Molecules are excited into $E_{\text{rot}} > 0$ states by ambient radiation and by collisions in a dense gas. The minimum gas temperature T_{min} needed for significant collisional excitation is

$$T_{\text{min}} \sim \frac{E_{\text{rot}}}{k} \approx \frac{\nu h(J+1)}{2k} \ . \tag{205}$$

7.7.3 Molecular Line Strengths

The electric dipole moment of a polar diatomic molecule with charges $+q$ and $-q$ is $|\vec{p}| \approx qr_{\text{e}}$. Each charge obeys the Larmor field Equation 36, so the total radiated electric field is

$$E_{\perp} = \frac{q(\omega^2 r_{\text{A}} + \omega^2 r_{\text{B}})\sin\theta}{rc^2}\exp(-i\omega t) \ , \tag{206}$$

the instantaneous power emitted is

$$P = \frac{2q^2}{3c^3}\omega^4 |r_{\text{e}}\exp(-i\omega t)|^2 \ , \tag{207}$$

and the time-averaged power is

$$\langle P \rangle = \frac{2q^2}{3c^3}(2\pi\nu)^4\frac{r_{\text{e}}^2}{2} = \frac{64\pi^4}{3c^3}\nu^4\left(\frac{qr_{\text{e}}}{2}\right)^2 = \frac{64\pi^4}{3c^3}|\mu|^2\nu^4 \ , \tag{208}$$

and the mean electric dipole moment is

$$|\mu|^2 \equiv \left(\frac{qr_{\text{e}}}{2}\right)^2 . \tag{209}$$

The spontaneous emission coefficient is

$$A_{\text{UL}} = \frac{\langle P \rangle}{h\nu} = \frac{64\pi^4}{3hc^3}|\mu_{\text{UL}}|^2\nu^3 \ , \tag{210}$$

where

$$|\mu_{\text{J}\rightarrow\text{J}-1}|^2 = \frac{\mu^2 J}{2J+1} \tag{211}$$

is the quantum mechanical value of μ_{UL} for the $J \rightarrow J-1$ transition. In convenient units,

$$\left(\frac{A_{J\rightarrow J-1}}{\text{s}^{-1}}\right) \approx 1.165 \times 10^{-11}\left|\frac{\mu}{\text{D}}\right|^2\left(\frac{J}{2J+1}\right)\left(\frac{\nu}{\text{GHz}}\right)^3 \ . \tag{212}$$

Here the dipole moment is given in units of debyes ($1\ \text{D} \equiv 10^{-18}$ statcoul cm).

For any molecular transition, there is a critical density defined by

$$n^* \approx \frac{A_{\text{UL}}}{\sigma v} \tag{213}$$

at which the radiating molecule suffers collisions at the rate $n^* \sigma v \approx n(\text{H}_2) \sigma v$ equal to the spontaneous emission rate A_{UL}. Typical collision cross sections are $\sigma \sim 10^{-15}$ cm^2 and the average velocity of the abundant H$_2$ molecules is $v \approx (3kT/m)^{1/2}$. The CO $J = 1 \rightarrow 0$ critical density is only $n^* \sim 10^3$ cm^{-3}, so CO emission is ubiquitous in galactic molecular clouds. Transitions with high emission coefficients (e.g., the HCN (hydrogen cyanide) $J = 1 \rightarrow 0$ line at $\nu \approx 88.63$ GHz has $A_{\text{UL}} \approx 2.0 \times 10^{-5}$ s^{-1}) are collisionally excited only at very high densities ($n^* \approx 10^5$ cm^{-3} for HCN $J = 1 \rightarrow 0$). They are valuable for highlighting the very dense gas directly associated with the formation of individual stars.

The line opacity coefficient

$$\kappa(\nu) = \frac{c^2}{8\pi\nu_0^2} \frac{g_{\text{U}}}{g_{\text{L}}} n_{\text{L}} A_{\text{UL}} \left[1 - \exp\left(-\frac{h\nu_0}{kT_{\text{x}}} \right) \right] \phi(\nu). \tag{214}$$

plus the column density $N_{\text{L}} \equiv \int n_{\text{L}} \, ds$ yield the line center opacity

$$\tau_0 = \int \kappa_0 \, ds = \frac{(\ln 2)^{1/2}}{4\pi^{3/2}} \frac{c^3}{\nu_0^3} \frac{g_{\text{U}}}{g_{\text{L}}} \frac{A_{\text{UL}}}{\Delta\nu} N_{\text{L}} \left[1 - \exp\left(\frac{h\nu}{kT_{\text{x}}} \right) \right]. \tag{215}$$

In the limit $h\nu \ll kT_{\text{x}}$ and $\tau_0 \ll 1$, the line brightness

$$\Delta T_{\text{b}} \approx (T_{\text{x}} - T_{\text{c}})\tau_0 = \left(\frac{T_{\text{x}} - T_{\text{c}}}{T_{\text{x}}} \right) N_{\text{L}} \frac{(\ln 2)^{1/2}}{4\pi^{3/2}} \frac{hc^3}{k\nu_0^2} \frac{g_{\text{U}}}{g_{\text{L}}} \frac{A_{\text{UL}}}{\Delta v} \tag{216}$$

is proportional to the column density N_{L}. The $^{12}\text{C}^{16}\text{O}$ line is often optically thick, but lines of rare isotopologues such as $^{13}\text{C}^{16}\text{O}$ are usually optically thin.

The fairly uncertain CO to H$_2$ conversion factor in our Galaxy is

$$X_{\text{CO}} = (2 \pm 0.6) \times 10^{20} \text{ cm}^{-2} \text{ (K km s}^{-1})^{-1}. \tag{217}$$

Neutral hydrogen gas in the disk of our Galaxy moves in nearly circular orbits around the Galactic center. Radial velocities v_r measured from the Doppler shifts of H I $\lambda = 21$ cm emission lines encode information about the *kinematic distances d* of H I clouds.

The H I line is an extremely useful tool for studying gas in the ISM of external galaxies and tracing the large-scale distribution of galaxies in the universe because H I is detectable in most spiral galaxies and in some elliptical galaxies. The Hubble distance to a galaxy with recession velocity v_r is $D \approx v_r/H_0$.

Beware the inconsistent "radio" and "optical" radial velocity conventions that were established when most observed radial velocities were much less than the speed of light.

Lecture 26:

7.8 The Neutral Hydrogen 21 cm Line

Neutral hydrogen (HI) atoms are abundant and ubiquitous in low-density regions of the ISM. They are detectable in the $\lambda \approx 21$ cm hyperfine line resulting from the magnetic interaction between the quantized electron and proton spins. When the relative spins change from parallel to antiparallel, a photon is emitted with frequency

$$\nu_{10} = \frac{8}{3} g_I \left(\frac{m_e}{m_p}\right) \alpha^2 (R_M c) \approx 1420.405751 \text{ MHz} , \qquad (218)$$

where $g_I \approx 5.58569$ is the nuclear g-factor for a proton, $\alpha \equiv e^2/(\hbar c) \approx 1/137.036$ is the dimensionless fine-structure constant, and $R_M c$ is the hydrogen Rydberg frequency (Equation 177).

The emission coefficient is

$$A_{10} \approx \frac{64\pi^4}{3hc^3} \nu_{10}^3 |\mu_B|^2 \approx 2.85 \times 10^{-15} \text{ s}^{-1} , \qquad (219)$$

where

$$|\mu_B| = \frac{e\hbar}{2m_e c} \approx 9.27401 \times 10^{-21} \text{ erg gauss}^{-1} \qquad (220)$$

is called the Bohr magneton. The low emission coefficient implies an extremely low critical density (Equation 213) $n^* \ll 1 \text{ cm}^{-3}$, so collisions can easily maintain this transition in LTE, even in the outermost regions of normal spiral galaxies and in tidal tails of interacting galaxies.

The HI line excitation temperature is called the spin temperature:

$$\frac{n_1}{n_0} \equiv \frac{g_1}{g_0} \exp\left(-\frac{h\nu_{10}}{kT_s}\right) , \qquad (221)$$

where the statistical weights of the upper and lower spin states are $g_1 = 3$ and $g_0 = 1$, respectively. Because $h\nu_{10}/(kT) \ll 1$ in the ISM,

$$\frac{n_1}{n_0} \approx \frac{g_1}{g_0} = 3 \qquad \text{and} \qquad n_H = n_0 + n_1 \approx 4n_0 . \qquad (222)$$

The opacity coefficient (Equation 191) of the HI line is

$$\kappa(\nu) \approx \frac{3c^2}{32\pi} \frac{A_{10} n_H}{\nu_{10}} \frac{h}{kT_s} \phi(\nu) , \qquad (223)$$

where n_H is the number of neutral hydrogen atoms per cm^3. The neutral hydrogen column density along any line of sight is defined as

$$\eta_H \equiv \int_{los} n_H(s) ds . \qquad (224)$$

The total opacity τ of isothermal H I is proportional to the column density. If $\tau \ll 1$, then the integrated H I emission-line brightness T_{b} is proportional to the column density of H I and is independent of the spin temperature T_{s} because $T_{\mathrm{b}} \approx T_{\mathrm{s}}\tau$ and $\tau \propto T_{\mathrm{s}}^{-1}$ in the radio limit $h\nu_{10}/(kT_{\mathrm{s}}) \ll 1$. Thus η_{H} can be determined directly from the integrated line brightness when $\tau \ll 1$. In astronomically convenient units it can be written as

$$\left(\frac{\eta_{\mathrm{H}}}{\mathrm{cm}^{-2}}\right) \approx 1.82 \times 10^{18} \int \left[\frac{T_{\mathrm{b}}(v)}{\mathrm{K}}\right] d\left(\frac{v}{\mathrm{km\ s}^{-1}}\right), \tag{225}$$

where T_{b} is the observed 21-cm-line brightness temperature at radial velocity v and the velocity integration extends over the entire 21-cm-line profile.

Beware that astronomers still use inconsistent radial velocity conventions that were established when most observed radial velocities were much less than the speed of light: the "radio" velocity for *any* v_r(radio) is

$$v_r(\mathrm{radio}) \equiv c\left(\frac{\nu_{\mathrm{e}} - \nu_{\mathrm{o}}}{\nu_{\mathrm{e}}}\right) \tag{226}$$

and the "optical" velocity defined for *any* v_r(optical) by

$$v_r(\mathrm{optical}) \equiv c\left(\frac{\lambda_{\mathrm{o}} - \lambda_{\mathrm{e}}}{\lambda_{\mathrm{e}}}\right) = cz, \tag{227}$$

where z is redshift.

If the H I emission from a galaxy is optically thin, then the integrated line flux is proportional to the neutral hydrogen mass

$$\left(\frac{M_{\mathrm{H}}}{M_{\odot}}\right) \approx 2.36 \times 10^5 \left(\frac{D}{\mathrm{Mpc}}\right)^2 \int \left[\frac{S(v)}{\mathrm{Jy}}\right]\left(\frac{dv}{\mathrm{km\ s}^{-1}}\right). \tag{228}$$

The total galaxy mass enclosed within radius r from its center is

$$\left(\frac{M}{M_{\odot}}\right) \approx 2.3 \times 10^5 \left(\frac{v_{\mathrm{rot}}}{\mathrm{km\ s}^{-1}}\right)^2 \left(\frac{r}{\mathrm{kpc}}\right), \tag{229}$$

where v_{rot} is the rotation velocity. The large total masses implied by H I rotation curves provided some of the earliest evidence for the existence of cold dark matter in galaxies. The empirical Tully-Fisher relation $L \propto v_{\mathrm{m}}$ between the luminosity L and maximum rotation velocity v_{L} provides distance that is independent of the Hubble distance and can be used to estimate the peculiar velocities of galaxies relative to the smooth Hubble flow.

The redshifted H I line traces the dark ages prior between recombination at $z \approx 1091$ and the reionization of the universe by the first stars and galaxies. The emission/absorption signals are very weak, but the potential scientific payoff of detection is so great that several groups around the world are developing instruments to detect them.

Lecture 27:

Spontaneous Emission and the Dark Energy Problem

Most of this course presented results from problems that have already been solved. For example, Planck solved the Rayleigh-Jeans "ultraviolet catastrophe" problem in 1905 by quantizing radiation into photons of energy $E = h\nu$. However, there are fundamental problems still waiting to be solved by the next Max Planck, maybe you. The most important unsolved problem in physics today is the discrepancy between spontaneous emission and the density of dark energy.

In 1916 Einstein proved that stimulated emission exists and derived the relation (*ERA* Equations 7.51)

$$\frac{A_{\mathrm{UL}}}{B_{\mathrm{UL}}} = \frac{8\pi h\nu_0^3}{c^3} \tag{230}$$

between the stimulated emission coefficient B_{UL} and spontaneous emission rate A_{UL} for a spectral line of frequency ν_0. He used only classical thermodynamics (the Boltzmann equation) and "old" quantum mechanics (the Planck blackbody radiation law and the relation $E = h\nu$ for photons). The classical Larmor formula could be used to approximate A_{UL} as a continuous radiation process, but in 1916 there was no quantum mechanical explanation for the spontaneous emission of a discrete photon.

What does "spontaneous" mean in physics anyway? Shouldn't everything have a cause? What makes an isolated atom in a perfect vacuum (so there is no stimulated emission) wait a certain amount of time $\sim A_{\mathrm{UL}}^{-1}$ and then suddenly decide to emit a photon?

Consider a single isolated hydrogen atom in intergalactic space where there are few Lyα photons. If its electron is orbiting in the $n = 2$ electronic energy level, we know that the electron will "spontaneously" emit a Lyα photon and drop to the $n = 1$ electronic ground state. The spontaneous emission rate for this process is $A_{2,1} \approx 6.3 \times 10^8$ s^{-1}; that is, a lonely but excited hydrogen atom typically takes only $\tau_{2,1} \equiv A_{21}^{-1} \approx 1$ nanosecond to emit a Lyα photon. Except in the rare case that a Lyα photon hits the hydrogen atom during that nanosecond, that emission is not stimulated emission.

As the quantum mechanics developed after 1916, it became clear that no emission can be truly "spontaneous" in a perfect classical vacuum. The stationary wave functions $|\psi_{\mathrm{U}}\rangle$ and $|\psi_{\mathrm{L}}\rangle$ describing the upper ($n = 2$) and lower ($n = 1$) electronic energy states of that hydrogen atom are orthogonal and have no overlaps $\langle \psi_{\mathrm{L}}|\psi_{\mathrm{U}}\rangle = 0$. The transition rate between orthogonal states is zero and no truly spontaneous emission can occur. Some perturbing Hamiltonian operator V is needed to make the perturbed states overlap so that $\langle \psi_{\mathrm{L}}|V|\psi_{\mathrm{U}}\rangle > 0$, thus allowing the electron to fall from $n = 2$ to $n = 1$ and emit a Lyα photon. In this quantum-mechanical picture, stimulated emission is easily understood: a Lyα photon hitting the $n = 2$ hydrogen atom provides the needed perturbation.

Thus quantum mechanics must treat *all* line emission as stimulated emission, and what appears to be "spontaneous" emission in a vacuum is actually stimulated by "virtual" photons of energy ΔE that appear briefly out of the quantum vacuum and vanish on time scales Δt consistent with the uncertainty principle $\Delta E \Delta t > \hbar \equiv h/(2\pi)$. Virtual photons may also account for the Casimir force attracting conducting plates and for Hawking radiation from black holes. Equation 230 determines the radiation energy density $\bar{u}$ and spectrum of the virtual photons. Equating the spontaneous emission rate A_{UL} to the stimulated emission rate $\bar{u}(\nu_0) B_{\mathrm{UL}}$ gives

$$A_{\mathrm{UL}} = \left(\frac{8\pi h \nu_0^3}{c^3} \right) B_{\mathrm{UL}} = \bar{u}(\nu_0) B_{\mathrm{UL}} \tag{231}$$

for a transition at frequency ν_0. Thus virtual photons in the quantum vacuum provide the spectral energy

$$\bar{u}(\nu_0) = \left(\frac{8\pi h \nu_0^3}{c^3} \right) \tag{232}$$

and the total radiation energy density u of the quantum vacuum needed to explain spontaneous emission at all frequencies ν is:

$$u = \int_{\nu=0}^{\infty} \bar{u}(\nu)\, d\nu = \frac{8\pi h}{c^3} \int_{\nu=0}^{\infty} \nu^3\, d\nu \ . \tag{233}$$

Note that this energy density u depends only on the immutable physical constants h and c; it does not change as the universe expands. In this sense, it acts like the dark energy that is currently accelerating the expansion of the universe. Unfortunately, like the Rayleigh-Jeans radiation energy density, the vacuum energy density in Equation 233 formally diverges. By analogy with the Rayleigh-Jeans "ultraviolet catastrophe," this has been called the "vacuum catastrophe."

Physicists have tried to tame the infinite u by setting a finite upper limit ν_{max} to the frequency or a lower limit to the wavelength λ_{min} for which the integration in Equation 233 can be meaningful:

$$u = \frac{8\pi h}{c^3} \int_{\nu=0}^{\nu_{\mathrm{max}}} \nu^3\, d\nu = \frac{2\pi h \nu_{\mathrm{max}}^4}{c^3} = \frac{2\pi hc}{\lambda_{\mathrm{min}}^4} \tag{234}$$

For example, no photon or other particle can have an energy greater than the Planck energy E_{P} defined by the requirement that two such photons do not form a black hole. A photon of energy E has a wavelength $\lambda = c/\nu = hc/E$ and mass $m = E/c^2$, so we set

$$E_{\mathrm{P}} = \frac{hc}{\lambda_{\mathrm{P}}} = \frac{Gm_{\mathrm{P}}^2}{r_{\mathrm{P}}} \tag{235}$$

and take $r_{\mathrm{P}} \approx \lambda_{\mathrm{P}}/(2\pi)$ as the "radius" of the particle to derive the Planck mass $m_{\mathrm{P}} = E_{\mathrm{P}} c^2$ at which the photon energy equals its gravitational potential energy:

$$m_{\mathrm{P}} = \left(\frac{\hbar c}{G} \right)^{1/2} \approx 2.18 \times 10^{-5} \ \mathrm{g} \ . \tag{236}$$

The Planck energy is very large for a photon ($E_P = m_P c^2 \approx 1.96 \times 10^{16}$ erg $\approx 1.22 \times 10^{19}$ GeV is comparable with the kinetic energy of a speeding freight train) and the Planck scale

$$l_P \equiv r_P = \frac{\hbar c}{E_P} = \frac{\hbar c}{(\hbar c/G)^{1/2} c^2} = \left(\frac{\hbar G}{c^3}\right)^{1/2} \approx 1.61 \times 10^{-33} \text{ cm} \tag{237}$$

is very small. The last four equations are unusual because they include both quantum mechanics and gravity, as indicated by the fact that they contain both h and G. There is still no quantum mechanics of gravity, so their meaning is uncertain. For example, is space continuous or quantized on scales $l_P \sim 10^{-33}$ cm?

Inserting $\lambda_P = \lambda_{\min}$ into Equation 234 gives

$$u = 2\pi \left(\frac{hc}{\lambda_P}\right) \frac{1}{\lambda_P^3} . \tag{238}$$

The quantity in parentheses is just the Planck energy E_P, and λ_P^3 is a volume, so u is an energy density. Its value is not infinite, but it is still an impossibly large $\sim 10^{113}$ erg cm^{-3}! Had u been this large, the universe would have collapsed immediately after the big bang.

Dark energy is observed to account for about 70% of the critical energy density $E_c = \rho_c c^2$ of the universe, where $\rho_c \approx 9.5 \times 10^{-30}$ g cm^{-3} for $H_0 = 71$ km s^{-1} Mpc^{-1} (*ERA* Equation 2.113), so the actual energy density of dark energy is only $u_{DE} \approx 6 \times 10^{-9}$ erg cm^{-3}. Equation 238 is a factor of $\approx 10^{121}$ higher, earning it the dubious honor of being called "the worst theoretical prediction in the history of physics." According to physics guru Steven Weinberg, "Dark energy is not only terribly important for astronomy, it's the central problem for physics. It's been the bone in our throat for a long time." Quantum gravity is not yet ready for prime time.

If supersymmetry (SUSY) theories are correct, the maximum frequency in Equation 234 might be lowered, but not nearly enough: the predicted vacuum energy density is still too high by a factor of $\sim 10^{57}$. The fact that u_{DE} is not exactly zero also suggests that the vacuum energy density is not exactly zero.

What is the maximum frequency $\nu_{\max}$ that is consistent with the observed energy density of dark energy? Solving Equation 234 for $\nu_{\max}$ and setting $u = u_{DE}$ yields

$$\nu_{\max} = \left(\frac{c^3 u_{DE}}{2\pi h}\right)^{1/4} \approx \left[\frac{(3 \times 10^{10} \text{ cm s}^{-1})^3 \cdot 6 \times 10^{-9} \text{ erg cm}^{-3}}{2 \cdot 3.14 \cdot 6.63 \times 10^{-27} \text{ erg s}}\right]^{1/4} \approx 1.40 \times 10^{12} \text{ Hz} \tag{239}$$

The rest frequency of the Lyα line (*ERA* Equation 7.13 with $n = 1$ and $\Delta n = 1$) is

$$\nu_0 = R_M c \left[\frac{1}{1^2} - \frac{1}{(1+1)^2}\right] = 3.28805 \times 10^{15} \text{ Hz} \times \frac{3}{4} \approx 2.47 \times 10^{15} \text{ Hz} , \tag{240}$$

much larger than the $\nu_{\max} \approx 1.40 \times 10^{12}$ Hz from Equation 239. The vacuum catastrophe is a problem even at infrared and optical spectral-line frequencies, so just tweaking $\nu_{\max}$ cannot avoid it.

Appendix C. Review of Special Relativity
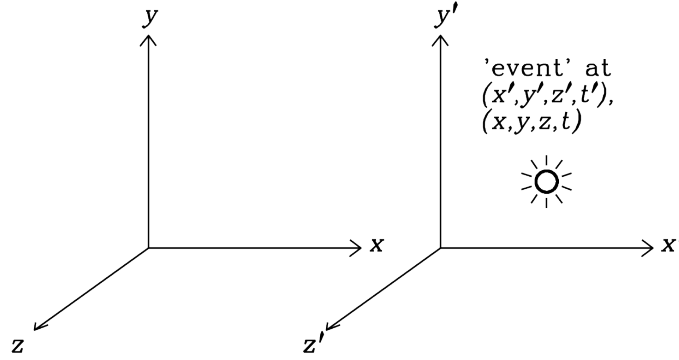
Galilean transform for primed frame moving with velocity $v = v_x$:

$$x = x' + vt' \qquad y = y' \qquad z = z' \qquad t = t \tag{241}$$
$$x' = x - vt \qquad y' = y \qquad z' = z \qquad t' = t \tag{242}$$

Lorentz transform:

Assume invariant speed c instead of $t = t'$. $c \to \infty$ gives Galilean transform. Assume space is homogeneous and isotropic. Then the Lorentz transform is

$$x = \gamma(x' + vt') \qquad y = y' \qquad z = z' \qquad t = \gamma(t' + \beta x'/c) \tag{243}$$
$$x' = \gamma(x - vt) \qquad y' = y \qquad z' = z \qquad t' = \gamma(t - \beta x/c) \tag{244}$$

where $\beta \equiv v/c$ and $\gamma \equiv (1 - v^2/c^2)^{-1/2} = (1 - \beta^2)^{-1/2}$. The differential Lorentz transform is

$$\Delta x = \gamma(\Delta x' + v\Delta t') \quad \Delta y = \Delta y' \quad \Delta z = \Delta z' \quad \Delta t = \gamma(\Delta t' + \beta \Delta x'/c) \tag{245}$$
$$\Delta x' = \gamma(\Delta x - v\Delta t) \quad \Delta y' = \Delta y \quad \Delta z' = \Delta z \quad \Delta t' = \gamma(\Delta t - \beta \Delta x/c) \tag{246}$$

Length contraction and time dilation by the Lorentz factor γ.

Velocity addition for particle with velocity $\vec{u} = (u_x, u_y, u_z)$ in the unprimed frame and $\vec{u'} = (u'_x, u'_y, u'_z)$ in the primed frame:

$$u_x = \frac{u'_x + v}{(1 + vu'_x/c^2)} \quad \text{and} \quad u'_x = \frac{u_x - v}{(1 - vu_x/c^2)} \tag{247}$$

$$u_y = \frac{u'_y}{\gamma(1 + vu'_x/c^2)} \quad \text{and} \quad u_z = \frac{u'_z}{\gamma(1 + vu'_x/c^2)} \tag{248}$$

$$u'_y = \frac{u_y}{\gamma(1 - vu_x/c^2)} \quad \text{and} \quad u'_z = \frac{u_z}{\gamma(1 - vu_x/c^2)} \tag{249}$$

Mass $m' = \gamma m$, energy $E' = m'c^2 = \gamma mc^2 = \gamma E$, power $P' = P$, charge $q' = q$